1997

Vortices incident upon an oscillating cylinder : flow structure and loading

Matthew A. Gaydon
Lehigh University

Gaydon, Matthew A.

Vortices Incident Upon an Oscillating Cylinder: Flow Structure and Loading

June 1, 1997

Vortices Incident Upon an Oscillating Cylinder: Flow Structure and Loading

by

Matthew A. Gaydon

A Thesis

Presented to the Graduate and Research Committee

of Lehigh University

in Candidacy for the Degree of

Master of Science

in

Mechanical Engineering

Lehigh University

May, 1997

This thesis is accepted and approved in partial fulfillment of the requirements for the degree of Master of Science.

04/29/97

Date

Professor Donald Rockwell
Thesis Advisor

Professor Charles Smith
Department Chairman

ACKNOWLEDGMENTS

I could not have possibly completed this journey here at Lehigh without the help and support of a great many people. First, I would like to thank my family at home, who were always there when I needed to get away. I would like to thank my brothers and sisters: Pat, Mike, Louise, Mary, Petie, and Little Lewie, and most of all Mom and Dad.

I would like to extend special thanks to Dr. Rockwell for his patience, support, and advice throughout the time I have spent at Lehigh. I must also extend special thanks to Dr. Knisely for his great assistance at Bucknell, for encouraging me to take this path, and for making this whole Lehigh experience possible.

Thanks are in order for all of my colleagues who have been in the fluids lab while I was here, expecially Dr. Lin and Oksan for their technical assistance as well as their friendship. I also want to extend thanks to Tom and Dan in P.L. 172 for all of their help and just for being there to help me keep my sanity. I cannot forget my officemates, Jin, Jong-Woo, and Bob Z., who were always there. I must thank my roommate Berk for his friendship and for helping with my classwork, and Pete for coming back to hang out on the weekends. The help of Frank and Emerson, Joann, and everyone else who made everything run smoothly in the lab is greatly appreciated. Dick Towne also deserves thanks for keeping the engines lab running and doing whatever he could to make my TA experience positive.

I would like to thank everyone in Goettingen for making my stay enjoyable, especially Markus for all of his assistance and for being a friend, Dr. Kompenhans for

making everything possible, and everybody at AIESAC-Goettingen and all of the other trainees for the unforgettable summer we spent together.

My friends from Bucknell who have stayed in touch and given me encouragement throughout the past two years deserve special thanks, especially my old roommates Toby, Los, and Digi. I'm sure we will continue to spend quality time together on the Central Pennsylvania trout streams.

Of course, I can't forget all of the guys from Muncy, with whom I've spent so many great times over the past 23 years: Brian, Brett, Bobby, Matt, Chet, Khan, and the rest of the crew from The Pine. I'm sure we will have many more great times together in the future.

Last, but not least, I must give very special thanks to Mary for everything she has done and been for me. I would not trade the times we shared for anything. Thank you for everything.

TABLE OF CONTENTS

LIST OF FIGURES

ABSTRACT

The flow structure around and subsequent loading on a cylinder in a vortex street is investigated experimentally. A laser scanning version of particle image velocimetry (PIV) is used to acquire quantitative snapshots of the flow field around the cylinder, while a strain gage assembly on a cantilevered cylinder is used to measure the lift and drag forces. The phase of the incident vortex street relative to the cylinder motion is controlled by changing the spacing between an upstream cylinder and the downstream cantilevered cylinder.

The measured value of fluctuating lift coefficient is shown to be an order of magnitude larger for the case with incident vorticity as compared to an isolated cylinder subjected to controlled oscillations in the absence of incident vorticity. The increase in fluctuating lift coefficient for the case with incident vorticity is accompanied by a significant shortening of the vortex formation length behind the cylinder. Two distinctly different states of interaction are shown to exist, depending upon the phase of the incident vortex street relative to the cylinder motion. One state exists in which the incident vortex passes to one side of the cylinder and merges with like-sign vorticity being shed from the cylinder. Another state exists in which the incident vortex impacts the cylinder and splits, with part of the vorticity passing to either side of the cylinder. It is also shown that the timing of the large-scale vortex formation in the near wake is controlled by the incident vorticity, rather than by the acceleration of the cylinder, as is the case for an isolated cylinder with uniform upstream conditions.

1.0 INTRODUCTION

Tandem cylinders in cross-flow is a common configuration associated with flow-induced vibration problems. Practical applications of this flow system include flow across heat exchanger tubes, piles of offshore platforms, bundles of transmission lines, and adjacent tall buildings. Obviously, cylinders in tandem are a very special case and cannot reveal the entire picture; however, generic aspects of the fluid-structure interaction and consequent loading of the structure, which are common to any arrangement, can be extracted from this simple arrangement.

Four mechanisms can account for the flow-induced vibration of cylindrical structures in tandem or staggered arrangements. The first mechanism is some upstream disturbance in the flow impacting the structure, and causing unsteady loading. This is commonly encountered when the structure is located in a turbulent flow field or if it is subject to gusts. The second mechanism is when the fluctuating fluid loading on the structure is due to an instability in the flow field which is inherent to the flow around the structure. Periodic vortex shedding behind a bluff body is a good example of this mechanism. The third mechanism is a movement-induced instability. This is a broad category, but an example of this can be seen in staggered arrangements in which there are vibrations due to the switching of a jet of fluid from within the cylinder gap to around one side of both cylinders. Acoustic resonance can influence all of the foregoing mechanisms. It occurs when system is contained in some finite space. An enclosed vessel will have a natural frequency at which standing waves will occur, which will cause

an unsteady loading of a structure within the flow. The most dangerous situation is when one or more of these mechanisms occur at a frequency that is close to the natural vibration frequency of the structure. Paidoussis (1981) provides a state of the art for vibrations of cylinders in cross-flow. He also includes a discussion of acoustic resonance and some of its practical consequences. More recently Ziada and Ongoren (1992, 1993) give a more in-depth look at acoustic resonance in their study of vortex shedding from an array of cylinders.

This study examines the influence of the vortices from an upstream cylinder impinging upon a downstream cylinder, and the manner in which the wake from the downstream cylinder is modified. More specifically the influence of the phase of the oscillatory motion of the downstream cylinder, relative to the impinging Karman vortex street, is investigated. High image density particle image velocimetry (PIV) is used in conjunction with force measurements, via strain gages measuring the moment on a cantilevered cylinder, in order to correlate the forces acting on the cylinder to the instantaneous pattern of the flow around it.

1.1 Single Cylinder

The case of flow past a single stationary cylinder has been studied since the late 1800's (Rayleigh, 1896). Bishop and Hassan (1964) provide a synopsis of some of these early studies, the most relevant to this study being that the frequency of the vortex shedding was a direct function of Reynolds number, and that the vibrations were greatly increased when the vortex shedding coincided with the natural frequency of the body.

Since Tritton (1959) reported that the Strouhal number (S = fd/U) vs. Reynolds number curve exhibited interesting behavior at Reynolds numbers below about 260, the majority of the literature has concentrated on this Reynolds number regime. Below this threshold Reynolds number the Strouhal number curve shows several discontinuities which are related to the onset of three-dimensionality in the wake of the cylinder. In the Reynolds number of interest in this study (Re = 700), the Strouhal number remains very constant at a value of about 0.21 with respect to Reynolds number. This means that the natural vortex shedding frequency increases linearly with flow velocity.

Another interesting point is that the vortex shedding is not always parallel to the cylinder axis for flow past a stationary cylinder. Williamson (1989) addressed the effect of end plates on the angle at which the vortices were obliquely shed from the cylinder, while Hammache and Gharib (1991) used control cylinders to change the upstream flow conditions, thereby controlling the vortex shedding in the wake of the test cylinder. For stationary cylinders, small perturbations in the flow system result in flow structures which are not coherent along the span of the cylinder. The result is that the loading inferred by examining the flow at one spanwise location does not necessarily represent that along the entire cylinder. At higher Reynolds numbers, such as that in this experimental investigation, the wake has three-dimensional structures such as vortices being shed in cells along the span of the cylinder. Once again, this would mean that the flow at one location is not always indicative of the flow at other locations.

1.1.1 Lock-on of Vortex Shedding

Relatively small oscillations of a single cylinder at a frequency close to the natural vortex shedding frequency predicted by the Strouhal number will result in locked-on vortex shedding from the cylinder. Lock-on may be defined as the shedding of phase-locked, spanwise coherent vortices at the same frequency as the cylinder oscillations. Richardson (1923) recognized the phenomenon of lock-on when he realized that the vortex shedding frequency varied from that predicted by the Strouhal relation over a range of flow velocities. It turned out that this variation occurred when the shedding frequency was close to the natural frequency of oscillation for the cylinder.

Mahir and Rockwell (1996) determined the frequency range over which lock-on occured for various oscillation amplitudes for a Reynolds number of 160. The results show that for a single cylinder, lock-on will not occur for oscillation amplitudes less than 0.1 cylinder diameters. The region of lock on broadens out from this point as the amplitude is increased. A practical simplification of their data would be that lock-on occurs over a shedding frequency range from about 80% of the natural frequency up to about 120% of the natural frequency for amplitudes greater than about 0.1 cylinder diameter. Williamson and Roshko (1988) performed experiments over a large range of amplitudes and frequencies of oscillation and classified the vortex shedding patterns. They defined two modes that can occur in the lock-on region: a mode having a form similar to the classical Karman street and a mode involving pairs of counter-rotating vortices.

1.1.2 Vortex Formation Length

Since Schiller and Linke pointed it out in 1933, it has been known that the vortex formation length changes dramatically over the range of Reynolds number from about 1,000 to 10,000. More recent investigations have shown that over this same range of Reynolds number there are also large changes in the mean base pressure coefficient and the fluctuating lift coefficient. Lin et al. (1995) used PIV to experimentally investigate this change in formation length. The results show that the formation length is close to its maximum at a Reynolds number of about 1,000 and shortens with increasing Reynolds number until the vortices are formed at the base of the cylinder at a Reynolds number of about 10,000. The resulting forces on the cylinder are strongly affected by this change in formation length. Alternating vortex formation at the base of the cylinder has a much greater effect on the fluctuating lift forces than when it occurs some distance downstream of the base of the cylinder.

It has been suggested by Lin et al. (1995) that the large scale vortex formation has its origin in the free shear layer with the Kelvin-Helmholtz instability and is not related to any vortical activity adjacent to the base of the cylinder. Small scale structures, known as Kelvin-Helmholtz (K-H) vortices, or in the bluff-body community as Bloor-Gerrard vortices, form in the range of Reynolds number from around 600 up to 1,900 depending on the free stream conditions. As the Reynolds number is increased these instabilities are amplified more quickly and result in a shortening of the vortex formation length. Chyu (1996) shows that very small amplitude (A/D ~ 0.001) oscillations of the cylinder at the

frequency of the Kelvin-Helmholtz instability, not only produces concentrated K-H vortices in the separated shear layer, but also a shortening of the formation length for the large scale Karman vortices. This can be considered further evidence that the formation of Karman vortices is very much dependent upon the instabilities in the shear layer as it separates from the cylinder. Chyu (1996) also shows that increasing the amplitude of this disturbance further decreases the vortex formation length.

Ongoren and Rockwell (1988) provide hydrogen bubble flow visualization of flow past a single cylinder, which provides some further insight into the issue of vortex formation length. For a Reynolds number of 885 flow visualization photographs are taken for five different ratios of excitation frequency to Karman vortex shedding frequency within the lock-on region. The visualizations show that there is a significant decrease in formation length for oscillation frequency ratios of 0.85, 0.90, and 1.0. For excitation frequencies above the Karman vortex shedding frequency, there is a switch in phase of the vortex shedding to the opposite side of the cylinder, and a further shortening of the vortex formation length with increased frequency.

1.2 Tandem Cylinders

A considerable amount of literature is available for many different multi-cylinder arrangements ranging from tandem cylinders to side-by-side cylinders and every possible arrangement between. Zdravkovich (1987) and Weaver and Fitzpatrick (1988) provide comprehensive reviews of the literature for tube bundles in cross flow. Tube arrangement geometry and the basic interference regimes for tandem cylinders are distinguished in the

work of Zdravkovich (1987). This provides a basis for qualitative interpretation and prediction of the forces exerted on a cylinder in a cluster. Weaver and Fitzpatrick (1988) note that, beyond the first few rows of a cylinder array, the periodic shedding becomes less coherent. It is also stated that grid turbulence further reduces the Strouhal response beyond the first few rows.

Zdravkovich and Pridden (1977) and Zdravkovich (1977) provide studies of the forces acting on tandem, side-by-side, and staggered cylinder configurations. These studies are primarily concerned with the fluid-elastic instabilities which commonly occur at higher Reynolds numbers ($Re > 10^4$). A map of the lift and drag coefficients for the downstream cylinder is provided for various locations with respect to the upstream cylinder by Zdravkovich (1977). From this map, the spacing at which the cylinders stop acting as one streamlined body and begin acting as two individual bodies can be deduced.

Kiya et al. (1980) provide some interesting insight into the vortex formation in the gap between cylinders in tandem and the influence of the upstream cylinder vortex shedding on the vortex shedding from the downstream cylinder. Various arrangements were tested for a Reynolds number of about 1.5×10^4. It was noted that no distinct vortices are formed in the gap when the spacing is less than about three cylinder diameters. Above this spacing the vortex shedding approaches that of a single cylinder. The vortex shedding behind the upstream cylinder strongly affects and synchronizes with the vortex shedding from the downstream cylinder.

Ziada and Ongoren (1992, 1993) studied the effects of vortex shedding and acoustic resonance in tube bundles. Velocity fluctuation amplitude distributions as well

as the coherence and phase relations across the wake and the jet flow between the cylinders in a square array are examined for intermediate and large cylinder spacings. Vortices were shown to form for cylinder spacings as small as 1.4 cylinder diameters. It is also interesting that the Strouhal number for tandem cylinders with large spacings is reported to be around 0.15 rather than the 0.21 which is well known for single cylinders at Reynolds numbers above about 260. A discontinuity is also reported for the Strouhal-Reynolds curve with a jump from 0.14 to 0.16. Upstream turbulence levels were shown to influence the location of this discontinuous jump.

Mahir and Rockwell (1996) investigated the flow characteristics for tandem cylinder systems with two different spacings. Gap widths of 2.5 D and 5.0 D were investigated at a Reynolds number of 160. The authors also found that the Strouhal number was about 0.15 for the closer cylinder spacing; however, the Strouhal number was about 0.19 for the cylinder spacing of 5.0 D. Plots of the region of lock-on were produced for both cylinder spacings, similar to their plot for the single cylinder. Once again, the lower amplitude limit for locked-on vortex shedding from the tandem cylinder system was about 0.1 cylinder diameters. For the cylinder spacing of 5.0 D the lock-on region is very similar to that of the single cylinder. The closer cylinder spacing produces much broader lock-on regions ranging from about 40% above and below the primary lock-on frequency. Another shift in the lock-on region is noted for the 2.5 D spacing depending upon whether the cylinders move in-phase or out-of-phase with each other.

1.3 Phase-Control of Fluid Loading

Several investigators have examined the effect of the relative phase of motion of a body and an incident vortex street on the loading of the body. The energy existing in the inflow is suspected to contribute to the efficiency of propulsion for marine creatures which propel themselves by oscillatory motion of lifting surfaces. The vorticity in the flow is harnessed by the motion of the caudal (tail) fin in order to optimize the thrust provided. Streitlien et al. (1994) used a two-dimensional, inviscid, numerical analysis of a heaving and pitching hydrofoil in a Karman vortex street to study these effects. They concluded that the propulsive efficiency can exceed 100% when the foil motions are on the order of half the vortex street width and the vortex street is strong enough to correspond to a drag coefficient of 0.4. Gopalkrishnan et al. (1996) experimentally investigated the same problem using a heaving and pitching foil in the wake of an oscillating D-shaped cylinder. Flow visualization experiments resulted in three basic modes of vortex interaction in the wake of the foil: 1) a street of vortex pairs forms with each pair consisting of a vortex from the cylinder and a vortex from the foil, 2) a street of vortices with lower or even opposite circulation than the original Karman vortex street (destructive interference), and 3) a similar vortex street with higher circulation than the original Karman vortex street (constructive interference). Force measurements showed peaks and troughs in the propulsive efficiency of the foil. It was concluded that the peaks are associated with mode 2 in which energy is actually extracted from the Karman vortex street, and the troughs are associated with mode 3 in which energy is lost to the incoming Karman vortex street.

Jefferies and Rockwell (1996) used PIV to experimentally investigate the alteration of vorticity formation by controlling the phase shift between an incident vortex and the motion of a leading edge. It was shown that the control of the phase shift is in fact an effective way to control the vorticity formation. The formation of a secondary vortex, which can significantly alter the fluctuating loading on the leading edge, can be eliminated if the relative phase of the motion is properly controlled.

1.4 Current Study

1.4.1 Scope

This experimental investigation focuses on the flow patterns and consequent loading on the downstream cylinder of a tandem arrangement. The phase angle of a downstream foil motion with respect to the incoming vortex street has been identified as the most important parameter based on the studies of Streitlien et al. (1994) and Gopalkrishnan et al. (1996). The current study includes tests for two cylinder spacings, and hence two relative phase angles, for tandem cylinders at a Reynolds number of about 700.

1.4.2 Objectives

The objectives of this study are to relate instantaneous flow patterns acquired via PIV to the corresponding force traces for tandem cylinder arrangements. It is desired to identify changes in the flow patterns and fluctuating forces acting on the downstream member of a tandem cylinder pair, related to the phase between the cylinder motion and

the incoming vortex street. It is hypothesized that there are 'peaks' and 'troughs' in the fluctuating lift coefficient similar to those found by Gopalkrishnan et al. (1996) for the efficiency of a foil performing pitching and heaving motion.

2.0 EXPERIMENTAL SYSTEMS AND TECHNIQUES

2.1 Flow System

Experiments were conducted in a recirculating, free-surface water channel located in the Lehigh University Fluid Mechanics Laboratory. The water channel test section is constructed of transparent Plexiglas for flow visualization purposes. The test section is approximately 1 m wide and 5 m long. The typical water depth for the present experiments is 0.540 m. Located upstream of the test section is a set of honeycombs and screens as well as a 2:1 contraction section to condition the flow. This flow conditioning provides low levels of turbulent intensity in the test section. A ten-inch axial-flow pump provides the driving force for the water channel. Flow speeds ranging from approximately 20 mm/sec to 380 mm/sec cam be attained in the test section. The current experiments were performed at a flow speed of 27 mm/sec corresponding to a Reynolds number of 700, based on a 25.4 mm diameter cylinder in cross-flow.

2.2 Experimental Apparatus

The experimental apparatus consisted of a 304.8 mm long 25.4 mm diameter cantilevered cylinder mounted in cross-flow approximately midway between the free-surface and bottom of the water channel (figure 2.1). The cylinder was mounted on a 3.175 mm square sting which was fitted with an arrangement of strain gages in order to measure the fluid loading on the cylinder (figure 2.2). Two 368 mm diameter circular endplates (6.4 mm thick with 30° outward bevel) were employed in order to reduce the

effects of the flow past the end of the cylinder. The gap between the end of the cylinder and the near endplate was kept at approximately 1 mm, such that the effects of the flow through the gap were minimized without being in contact with the cylinder. Slots were cut in the endplates such that a second cylinder could be mounted directly upstream of the test cylinder. The slots allowed a continuous range of cylinder spacings from a minimum of 110 mm to a maximum of 163 mm. A laser window was machined into the test cylinder to minimize the shadow and distortion of the PIV laser sheet as it passed through the cylinder. This was done by machining very thin walls in a small section of the cylinder and filling the section with distilled water in an effort to match the refractive index of the cylinder to that of the water. This window was 12.7 mm in length and was located 101.6 mm from the end of the cylinder.

In the present study, small amplitude oscillations of the entire apparatus normal to the flow direction were used to attain locked-on vortex shedding. Figure 2.3 shows the configuration of the experimental apparatus, computer control, and photographic equipment. The oscillation frequency that was used was 0.21 Hz which corresponds to a Strouhal number of 0.21. The amplitude of the oscillation was A/D = 0.125 which is sufficient to provide lock-on (Mahir and Rockwell, 1996). The motion was provided by a high resolution stepper motor (Parker Compumotor AX57-102) which has an angular resolution of 25,000 steps per revolution. The stepper motor is controlled via a Parker PC-23 indexer and two in-house developed software programs. The software Stream Function Generator (SFG) (Magness, 1990) was used to produce a profile that specifies the motor displacement for each discrete time step. The Automated Lab Technician

(ALT) (Magness and Troiano, 1991) executes the SFG commands for up to three stepper motors and allows for simultaneous data acquisition through a Data Translation (DT 2801 series) A/D converter. Additionally, commands were embedded within the SFG profile to command the 35 mm camera and the rotating bias mirror used for particle image velocimetry (PIV) image acquisition. The same signal that was used to trigger the first camera shutter opening was also used to trigger the acquisition of the forces from the strain gage assembly.

2.2.1 Strain Gage Assembly

The cantilevered strain gage sting (figure 2.2) was constructed by Edward Tomlinson of ATLSS Instrumentation. The sting is constructed of 3.175 mm square brass stock and has one strain gage (Measurements Group, Inc.; EA-13-125BT-120) mounted on each face in order to discern the lift and drag components of the fluid loading. The strain gages were to be submerged in the water channel, so special care was taken to be sure that they were waterproof. All details of the strain gage sting are documented in *Strain Gage Stings* (Tomlinson, 1996).

The force data were acquired with the same ALT program that was used to control the motion of the stepper motors. The force signal passed through an analog filter (Krohn-Hite 3750) which operated in the low-pass mode with a cut-off frequency of 4 Hz, and the gain was set at 20 dB. ALT acquired the data through a Data Translation DT-2801 series A/D converter. The A/D converter was set at a gain of 8, and a total of 4,096 data points were acquired at a Nyquist frequency of 200 Hz.

Some precautions are advised for the use of the strain gage force measurement device. The zero level of the output voltage must be carefully adjusted and should not be done until the system has been allowed to warm up for several minutes in a quiescent fluid. A simple check will also determine the polarity of the voltage signal and can help to avoid problems later in the data analysis phase. Additionally, a standard test should be performed to check the calibration of the strain gages. The cylinder should be oscillated at several Keulegan-Carpenter numbers ($2\pi A/D$) and the drag coefficient should be checked against the published results of Bearman et al. (1985): $C_{Frms} = (2\pi^2/KC)^{0.5}$. For these experiments KC numbers of 1 and 10 were used and the output voltage was obtained by visually examining the trace on an oscilloscope. These tests agreed with Bearman et al. (1995) to within approximately 10%. A static calibration was performed for this particular strain gage sting by hanging weights from the end of the cylinder (Cetiner, 1996) and the following relation was derived for the force coefficient in the lift direction:

$$C_l = -0.2174 * \frac{V}{U^2}$$

Where V is the actual voltage from the strain gages (corrected for any gain added in the filter) and U is the free stream velocity in m/s. It was assumed that any fluid force acting on the cylinder was perfectly distributed along the span of the cylinder. Note that this is the actual fluctuating lift coefficient, the rms fluctuating lift coefficient can be obtained by multiplying this by 0.707. For the strain gage configuration in the present apparatus,

the polarity of the lift force is negative meaning that an upward force results in a negative voltage. A drag force in the downstream direction results in a positive voltage.

2.3 Laser Scanning and Image Acquisition

A laser scanning version of particle image PIV was used to provide quantitative flow visualization. PIV provides a high spatial resolution two-dimensional instantaneous velocity field. From this velocity field, other flow characteristics can be calculated such as vorticity concentrations, streamline trajectories, Reynolds stresses, etc. Comprehensive reviews of the PIV technique are presented by Landreth and Adrian (1988), Adrian (1991), and Rockwell et al. (1993).

The laser sheet is created using the laser-optical apparatus described by Corcoran (1992). A continuous Argon-ion laser (Coherent Innova series) with a maximum power output of 30 watts was used in conjunction with either a 72-facet rotating mirror, specially modified for low rotational speeds (Lincoln Laser Co., model M660-010-LVWOB, serial number 9510690A), or an oscillating mirror (General Scanning, Inc.) to create the laser sheet approximately 1 mm thick. The flow was seeded with silver coated, hollow glass spheres (Conduct-O-Fil made by Potters Industries, Inc.) with an average diameter of 14 microns and a density of 1.65 gm/cc. These particles are very close to being neutrally buoyant, and for the time scales used in these experiments the particles were considered to follow the flow to within the accuracy of the PIV technique.

For the test in which the oscillating mirror was used to create the laser sheet, the scanning frequency was 80 Hz. This was determined to be the maximum possible

frequency without getting a second particle image from the return of the mirror to its original position. The rotating mirror was operated at approximately 1.5 Hz, resulting in a scanning frequency ($f_{sc} = 72\ f_m$) of 108 Hz for the present experiments. The motor driving this mirror was specially wound for low frequencies, and a sweep function generator (Heath Co. SG-1274) was used to provide a high precision square wave to drive the motor; however, some unsteadiness was still noticed in the laser scanning rate. A possible solution to this problem would be to use a rotating mirror with fewer facets (~8-10 facets), so that a higher motor frequency could be used to produce the same scanning frequency.

The flow field illuminated by the laser sheet was captured photographically on 35 mm Kodak TMAX 400 film with a Canon EOS-1 N RS camera and a 100 mm telephoto lens. A camera shutter speed of 1/25 and f-stop = 9 were used for these experimental cases. At a shutter speed of 1/25, the maximum framing rate of the camera was determined to be around 6.5 Hz. The use of ALT required that the camera be triggered at one of the discrete time steps (every 12 ms in this case), so the time between camera shots was 156 ms corresponding to a framing rate of 6.4 Hz. At this framing rate nearly 31 frames could be taken during one cycle of the cylinder motion (T=4.75 sec) providing a quite high time resolution ($\Delta T/T \sim 0.033$).

The PIV images in this experiment were primarily of the separated wake behind the downstream cylinder which included a large region of back flow. An artificial 'bias' velocity was added to each image to eliminate this directional ambiguity (Adrian, 1986). This bias was added using a 45 degree rotating mirror between the camera and the laser

sheet. Not only did this bias remove the directional ambiguity of the flow, but it also decreased the dynamic range to allow better interrogation of the flow field. In these experiments, the frequency of the ramp signal sent to the bias mirror was kept constant at 10 Hz. The amplitude was varied in order to determine the optimum particle spacing on the film. The resulting optimum amplitude of the ramp signal was experimentally determined to be 0.125 V. This provided an actual bias velocity of about 3 times the average flow velocity in the streamwise direction.

Raffel and Kompenhans (1995) discuss systematic errors that can arise with the use of a rotating mirror to produce image shifting for the removal of directional ambiguity. The result is that the bias velocity varies with location in the image. This error is most significant with large rotation angles during the exposure period and with large magnification factors. The location of the rotating mirror also has a large effect on this error. The error is largest when the rotating mirror is located close to the laser sheet. In this investigation the mirror is located at the maximum possible distance from the laser sheet and rotated less than 1° in a period of 100 ms. The camera shutter was open for only 40 ms which further decreased this error. It has been assumed that this error is negligible with respect to all other uncertainties associated with the PIV technique for this study.

With the proper choice of bias parameters, laser scanning frequency, and camera shutter speed, multiple images of individual particles are present on the film negative. The spacing between these particle images is proportional to the vector sum of the local and bias velocities. The next section will describe the process of interrogating the

negatives to produce this velocity data.

2.4 Image Processing and Interrogation

The photographic negatives were digitized at a resolution of 125 pixels/mm using a Nikon LS-3510AF 35 mm film scanner, and each image was stored in Transferable Image File (TIF) format. In-house developed software (PIV3; Seke, 1993) was used to interrogate the images in order to extract the average particle image spacing for smaller windows within the flow field. A single-frame, cross-correlation (Keane and Adrian, 1992) was performed on each window (80 pixels x 80 pixels) resulting in an average displacement for each window. Successive windows were overlapped by 50% in order to smooth the data, resulting in a grid size of 40 pixels x 40 pixels (0.32 mm x 0.32 mm in the film plane). This grid size in the film plane corresponds to a grid size of approximately 1.4 mm x 1.4 mm in the real flow plane. Another program called TRACETIF (Image Alchemy, 1992) was used in conjunction with BOUND2 (Lin, 1996) to trace the outline of the cylinder in the TIF file.

The resulting displacement vector field and the cylinder boundary were then viewed using V3 (Robinson, 1992). Outliers or bad vectors can be identified by the user and removed from the vector field. These outliers are most prevalent in areas near to the cylinder where the laser reflection distorts or hides the particle images, or in the shadow of the cylinder where the laser sheet is not uniform. Outside of these two regions, the interrogation was nearly perfect with much less than 1 % of the vectors being outliers. This program was also used to calculate streamlines for the flow field.

Following this process of cleaning the displacement vector field, an in-house developed program called NFILV (Lin, 1994) was used to interpolate values for the areas in which the vectors had been removed. NFILV also uses the magnification factor, laser scanning rate, and bias displacement to calculate actual velocities from the particle image displacements. The interpolated velocity field was also smoothed using a Gaussian weighted average technique described by Landreth and Adrian (1988), with a Gaussian smoothing parameter of 1.3. In addition the out-of-plane vorticity component was calculated and displayed using SURFER (Golden Software, Inc., 1989).

2.5 Experimental Cases

In order to control the relative phase between the incoming vortex street and the downstream cylinder motion,the cylinder spacing was varied. The convective velocity of the vortex street does not vary with spacing; however, the time required for the shed vortices to travel the greater distance accounts for the phase shift.

At a Reynolds number of 700, four different experimental test configurations were used. Preliminary experiments on the tandem cylinder arrangement allowed determination of the cylinder spacings that resulted in maximum and minimum fluctuating lift forces on the downstream cylinder (minimum force at L = 113 mm, maximum force at L = 155 mm). Simultaneous PIV and force measurements were later taken at these two spacings. For comparison, similar data were also acquired for cases involving a single stationary and single oscillating cylinder. For all cases involving cylinder oscillations, the cylinder system was oscillated at the frequency of natural vortex

shedding with a dimensionless amplitude of A/D = 0.125.

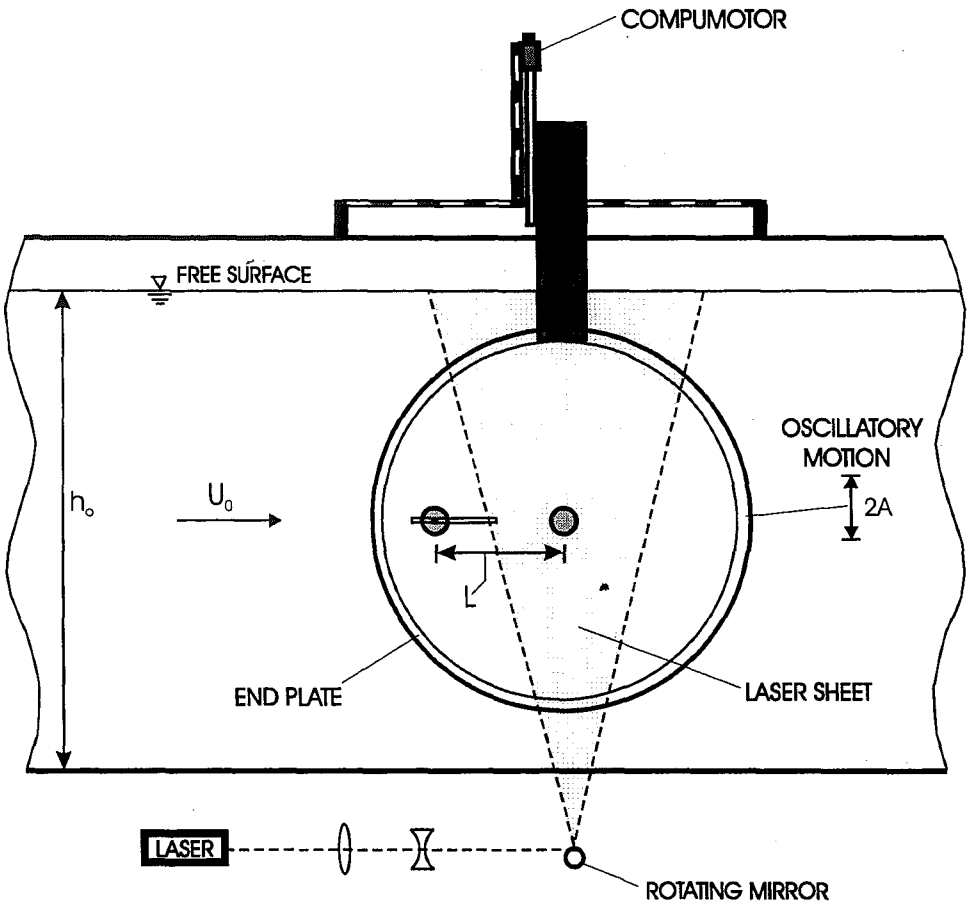

Figure 2.1 Schematic of the experimental apparatus and the PIV field of view.

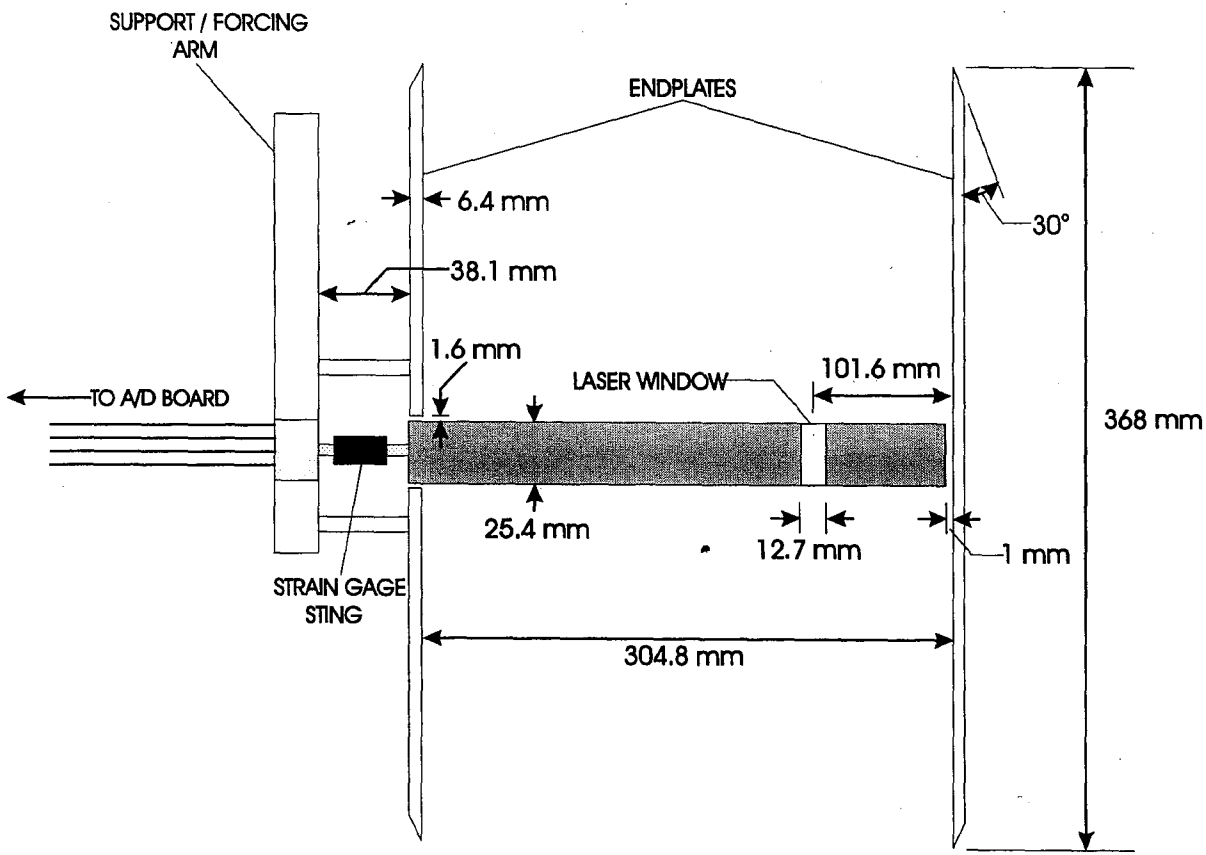

Figure 2.2 Detailed schematic of cantilevered cylinder used to measure fluid loading.

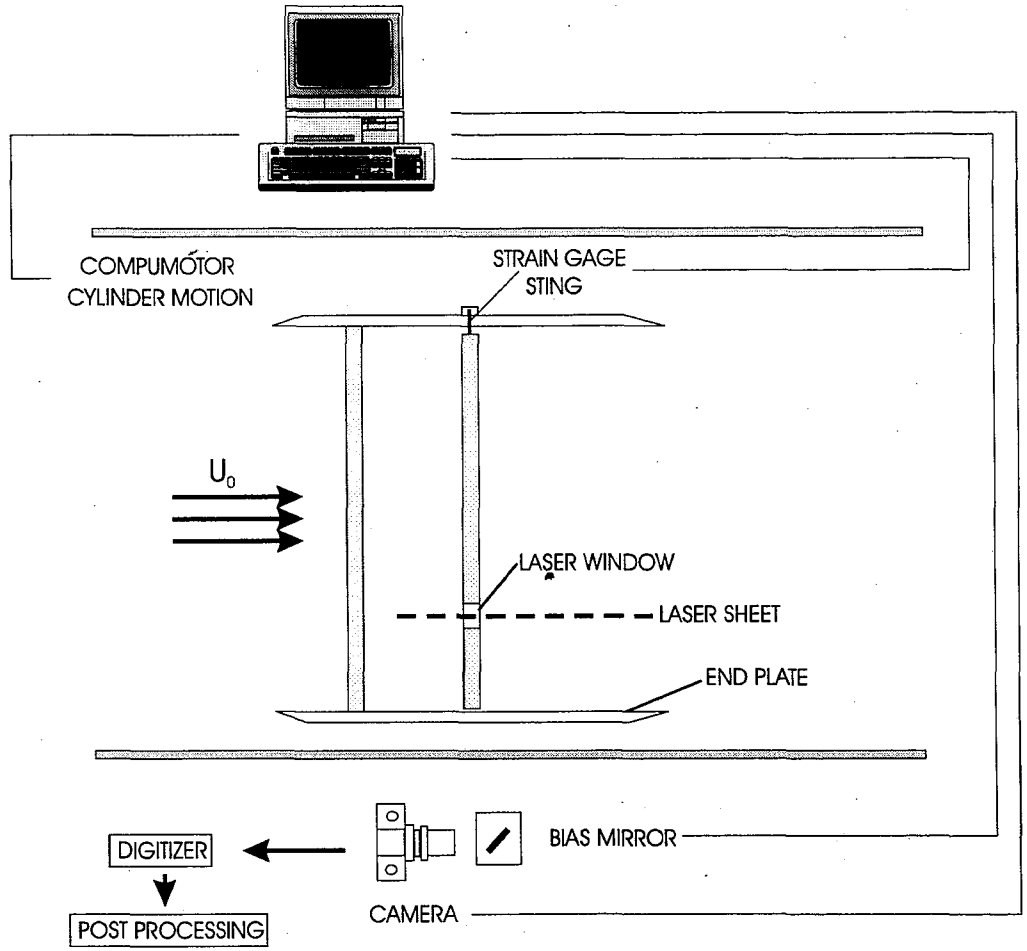

Figure 2.3 Configuration of experimental apparatus, computer control, and photographic equipment.

3.0 RESULTS

Using the studies of Jefferies and Rockwell (1996), Gopalkrishnan et. al. (1994), and Streitlien et. al. (1996) as a guideline, it was hypothesized that by changing the relative phase between the incident flow and cylinder motion, the loading on the downstream cylinder could be altered. In the present study, this phase is varied by changing the distance between cylinders in a tandem arrangement. Comparisons of the flow structure and loading are made among single stationary and oscillating cylinder cases (no incident vortices), and tandem cylinder cases (incident vortices) at two different cylinder spacings.

The vorticity contour maps, streamline plots, and velocity vector plots are referenced according to the PIV frame number, which in turn is related to a defined phase of the cylinder motion. Figure 3.1 provides this information, using different data symbols corresponding to different comparisons of single and tandem cylinders, which will be explained for the relevant images.

3.1 The Experiment

3.1.1 Lock-On

Due to the complex nature of the flow and the three-dimensionalities present in the flow field, lock-on cannot be so cleanly attained for a tandem cylinder arrangement as for a single cylinder. Lock-on is characterized by spanwise coherent vortices being shed

from the cylinder and by structures in the wake being phase-locked with the cylinder motion. Initially, dye visualization was used to qualitatively verify that the vortex formation was coherent along the span of the cylinder and phase-locked with the cylinder motion. Unbiased images of the flow field were also used to check the phase-locked condition of the downstream cylinder wake. These techniques showed that, even at the lock-on frequency, there are small variations in the structure of the wake. The periodicity of the lift and drag coefficient traces for the downstream cylinder was also examined as a criterion for determining lock-on. Once again, small fluctuations were unavoidable even at the lock-on frequency. Figures 3.2, 3.3a and 3.3b are plots of the measured fluctuating lift and drag coefficients as a function of time for the two cylinder spacings investigated. These traces clearly show some modulations which are an indication of the difficulty of producing perfectly locked-on vortex shedding.

3.1.2 Vortex Formation Length

At the Reynolds of 700 in these experiments, the vortex formation behind a single cylinder occurs well downstream of the base of the cylinder (figure 3.4). A vortex formation length on the order of 2-3 cylinder diameters was found for the single cylinder measurements in this experiment, which roughly agrees with Lin et. al. (1995) for a Reynolds number of around 1000, and with Ongoeren and Rockwell (1988) for a Reynolds number of 885. The formation length can change somewhat in this range of Reynolds number depending on factors such as upstream flow conditions, so exact agreement cannot be expected. It is also shown by Ongoren and Rockwell (1988) that

within the lock-on frequency range, slight variations in oscillation frequency can cause subtle changes in vortex formation length.

3.1.3 Motivation

A quick comparison of the lift force trace corresponding to the incident vortex cases (figure 3.3a) with the no incident vortex (figure 3.3b) shows an increase in fluctuating lift coefficient ranging from 500% to 1000%. The primary motivation behind this study is to gain insight into the flow physics associated with this dramatic increase in fluctuating lift coefficient.

3.2 Single Cylinder Comparison (No Incident Vortex)

3.2.1 Flow Images

Figure 3.4 shows contours of constant vorticity, streamline patterns, and velocity vector plots for the no incident vortex cases (single stationary and oscillating cylinder). The streamline patterns and velocity vector plots are in a reference frame moving at 70% of the freestream velocity. The images for the case of the stationary cylinder had no cylinder motion associated with them to use to synchronize images with other cases, so a trial-and-error process was used to select an image that matched the phase of the image chosen for the oscillating cylinder. These two cases are remarkably similar in almost all respects; however, several subtle differences can be noted. The wake of the oscillating cylinder seems to swing back-and-forth with the cylinder motion, and the vortices formed in the wake of the oscillating cylinder are also distorted in shape somewhat from the

predominantly circular vortices formed from the stationary cylinder.

3.2.2 Lift Coefficient

The amplitude of the fluctuating lift coefficient shows a modest increase for the case of the single oscillating cylinder as compared to that of the single stationary cylinder (figure 3.3b). The fluctuating lift coefficient for the single stationary cylinder is small and barely measurable above the electronic noise that is unavoidable in the measurements. One possible explanation for the small magnitude of these measured lift coefficients is that the vortices may not have been shed coherently along the entire cylinder. The relatively long formation length of the vortices also indicates that the force induced by the vorticity formation would be minimal (Lin et al., 1995).

The fluctuating lift force for the single oscillating cylinder was much more regular than that for the stationary cylinder. This could be due to the better spanwise coherence of the vortex shedding from the cylinder. The lift coefficient was also calculated for the theoretical added-mass force, and was found to be on the same order of magnitude and of the same sense as the measured lift coefficient. Although the flow is separated, this can still be used as an approximation of the actual added-mass component of the lift coefficient. In light of this, the force induced by the vorticity would account for only a small part of the total lift coefficient.

3.3 Tandem Cylinder Comparison (Incident Vortex)

Two different cylinder spacings were used to attain a phase difference of

approximately 180 degrees for the two incident vortex configurations. It should be noted that the 180 degree phase difference is based upon the phase of the cylinder motion relative to the incident vortex street. A trial-and-error process was used to determine precisely which spacings to use by examining the force traces for several spacings between 110 mm and 163 mm. Cylinder spacings of L = 113 mm and L = 155 mm (figure 1.2) were chosen because they produced extreme fluctuating lift force amplitudes. The PIV images later verified that the incident vortices were approximately 180 degrees out of phase for these two cases. Cylinder spacings less than about 110 mm were not considered because the downstream cylinder would begin to interfere with the vortex formation from the upstream cylinder.

Some of the terminology that will be used in the following sections will be explained here. The two tandem cylinder cases will be called $\Phi_v = 0°$ (L = 113 mm) and $\Phi_v = 180°$ (L = 155 mm) coinciding with the arrival of the positive or negative incident vorticity. The vorticity coming from the upstream cylinder and impinging upon the downstream cylinder will be referred to as 'incident vorticity', while the vorticity being shed from the downstream cylinder will be referred to as 'shed vorticity'. The individual vortices are labeled A through F (figure 3.5) to make it easier to trace their movement from one frame to the next.

3.3.1 Vortex Formation Length

Figures 3.5 and 3.6 are vorticity contour maps and streamline patterns for frames 8, 12, 16, and 18 (filled triangles in figure 3.1) for the two incident vortex cases. In each

of these figures, the images in the left and right columns correspond to exactly the same phase of the cylinder motion. The streamline patterns are in a reference frame moving at 70% of the free stream velocity. Comparing these images to those for the single cylinder cases, it is apparent that the upstream flow conditions have a great effect on the vortex formation length in the wake of the downstream cylinder. For both incident vortex cases, the vortices form very close to the base of the downstream cylinder. In contrast, the vortices form two to three diameters away from the base of the cylinder for the no incident vortex cases (figure 3.4).

Lin et. al. (1995) report that for a stationary cylinder, the fluctuating lift coefficient increases from about zero at a Reynolds number of around 1,000 to around 0.4 at a Reynolds number of 10,000. The same study shows that the vortex formation length is quite long at Re = 1,000 and shortens as the Reynolds number approaches 10,000. From this it can be inferred that as the vortices form closer to the base of the cylinder, they have a greater effect on the cylinder loading. In this experimental case, the incident vortical flow causes a shortening of the vortex formation length in the wake of the downstream cylinder (see figure 3.5), which in turn is accompanied by a substantial increase in the fluctuating lift coefficient (figures 3.3a and 3.3b).

3.3.2 Phase of Incident Vortex

By comparing vorticity contour maps for the $\Phi_v = 0^\circ$ (figure 3.5, left column) and $\Phi_v = 180^\circ$ (figure 3.5, right column) cases, it is apparent that the incident vortices (E) are approximately 180 degrees out-of-phase with respect to each other. In the sequence for

the $\Phi_v = 0°$ case, vortex E, of negative sense and having come from the top side of the upstream cylinder, can be seen approaching and impacting the downstream cylinder. In the corresponding images for the $\Phi_v = 180°$ case, vortex E can also be seen approaching and impacting the cylinder. In this case however, vortex E is of positive sense and came from the bottom side of the upstream cylinder. This would indicate that vortex E, for the $\Phi_v = 180°$ case, was shed one half cycle later in the cylinder motion producing the 180 degree phase shift.

3.3.3 Phase of Shed Vorticity

The shed vorticity in the wake of the downstream cyinder exhibits a dramatic phase change for the $\Phi_v = 180°$ case, relative to that of the $\Phi_v = 0°$ case and the single cylinder case. This can be seen best by comparing the streamline patterns in figure 3.6 with those for the single cylinder at the same phase (figure 3.7). The wake in the $\Phi_v = 0°$ case appears to be very close in phase to that of the no incident vortex case. Looking at the vorticity contours, it can be seen that in frame 8 for both the $\Phi_v = 0°$ and no incident vortex cases, a negative vortex (A, figure 3.5) is shed from the top of the cylinder, while a positive vortex (B) is rolling up from the bottom of the cylinder towards the centerline of the wake. The opposite is true for the $\Phi_v = 180°$ case, for which a positive vortex (A) is shed from the bottom of the cylinder, and a negative vortex (B) is rolling up from the top of the cylinder towards the centerline of the wake.

This is fairly convincing evidence that the phase of the vortices being shed is

controlled by the incident vorticity. This is contrary to the single cylinder case, in which the acceleration of the cylinder controls the phase of the shed vorticity as described by Williamson and Roshko (1988).

3.3.4 Incident Vortex - Cylinder Interaction

Referring to figure 3.5, two distinctly different interactions can be seen to occur between the incident vortex (E) and the cylinder. For the $\Phi_v = 0°$ case, the incident vortex retains its identity throughout the sequence, even after impacting the cylinder (frames 16 and 18). On the other hand, for the $\Phi_v = 180°$ case, the incident vortex splits upon impacting the cylinder. Most of its vorticity is destroyed by interactions with the vortical structures being formed in the boundary layers along the sides of the cylinder. It can be seen from images 12 through 18 that vortex E breaks up and has almost completely lost its identity.

Another illustration of these two states of interaction can be seen in figure 3.8. These two frames do not correspond to the same phase in the cylinder motion (frame 22 for the $\Phi_v = 0°$ case and frame 17 for the $\Phi_v = 180°$ case; open squares in figure 3.1); however, they were chosen to demonstrate the size of the large negative vortices that result from the merging of incident and shed vorticity. The dimensionless circulation for the large vortices in these two cases reflects the vortex interactions that have been described above. For the $\Phi_v = 0°$ case, the dimensionless circulation ($\Gamma^* = \Gamma/\pi UD$) was determined to be -1.22 for the contour defined by $\omega = -2\ s^{-1}$. Using the same vorticity

level contour to define the boundary of the large negative vortex for the $\Phi_v = 180^o$ case, the dimensionless circulation was determined to be -0.80.

3.3.5 Drag Coefficient

Comparing figures 3.2 and 3.3a gives some perspective on the magnitude of the drag and lift forces present in the tandem cylinder arrangement. The fluctuating drag coefficient is an order of magnitude smaller than the fluctuating lift coefficient, so the characteristics of the lift coefficient were of primary interest in this study. As would be expected, the drag coefficient is quasi-periodic at twice the frequency of the cylinder oscillation. The smaller magnitude of the drag force measurements made them more sensitive to electronic noise as well.

3.4 Phase Diagrams

Figures 3.9 and 3.10 are phase diagrams for the lift coefficient as a function of position for the incident vortex and no incident vortex cases. These diagrams consist of data from three or four force traces of two oscillation cycles per trace. Figure 3.11 consists of phase diagrams for the drag coefficient for the two incident vortex configurations. For figure 3.11, data from only one force trace was used for each diagram, and the two cycles are offset from each other to make it easier to trace the trajectories. The dashed lines indicate the zero level of the fluctuating drag coefficient for each case. Arrows have been drawn in on all phase diagrams so that the trajectories can be traced.

3.4.1 Lift Phase Diagrams

Figures 3.9 and 3.10 show that the trajectories of the phase diagrams form closed loops with some net area enclosed within the loop. The direction in which the trajectories are traversed indicates the direction of the energy transfer in the system. A clockwise trajectory indicates energy being transferred from the fluid to the body and vice-versa (Naudascher and Rockwell, 1994). It can be seen that the $\Phi_v = 0°$ and no incident vortex cases do have clockwise trajectories, while the trajectory is counterclockwise for the $\Phi_v = 180°$ case. Considering the relative phases of the shed vorticity for the two incident vortex cases and for the no incident vortex case (figures 3.5 and 3.7), it makes sense that the $\Phi_v = 0°$ case and the single oscillating cases have similar trajectories and that the $\Phi_v = 180°$ case is different. This also reinforces the idea that the viscous loading on the cylinder is primarily caused by the vorticity being formed in the wake of the cylinder, rather than by the incident vorticity impacting the cylinder.

3.4.2 Drag Phase Diagrams

The phase diagrams for the drag force (figure 3.11) show several differences between the $\Phi_v = 0°$ and $\Phi_v = 180°$ cases. One difference is that the distorted figure-eight shaped trajectories are more-or-less mirror images of each other. This can most likely be attributed to the 180 degree difference in the phase of the shed vorticity for these two cases. Another difference is that for the $\Phi_v = 180°$ case, the trajectory has an additional loop on the right side. This additional loop could be due to an irregularity in the vortex

shedding in the wake of the cylinder for the $\Phi_v = 180^o$ case.

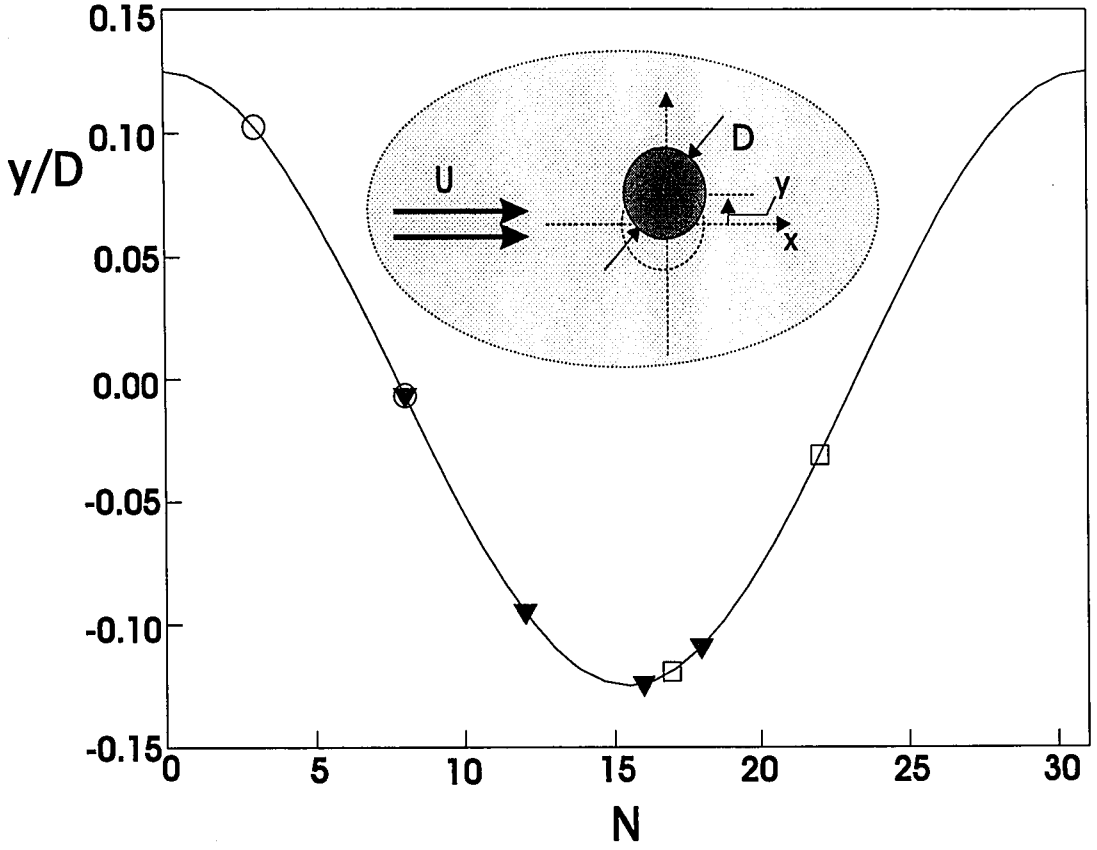

Figure 3.1 Location of relevant frame number with respect to cylinder position.
○ = Frames for no incident vortex case
▼ = Frames for incident vortex cases
□ = Frames for comparison of large vortices for incident vortex case

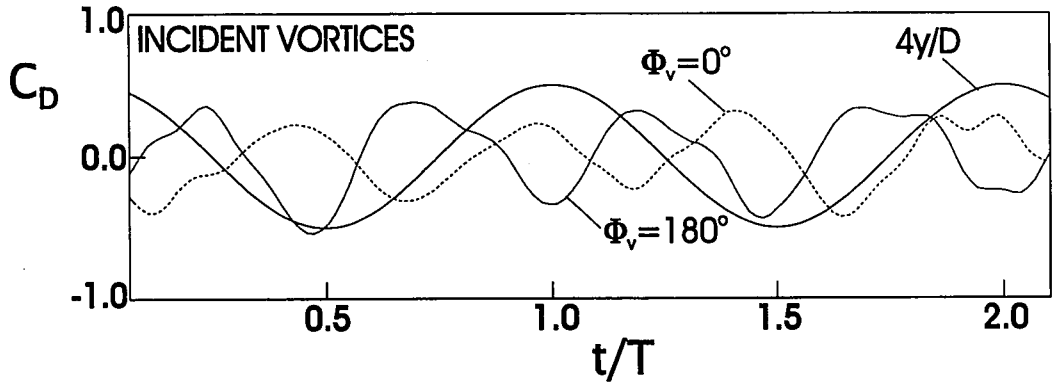

Figure 3.2 Drag coefficient as a function of time for the incident vortex case.

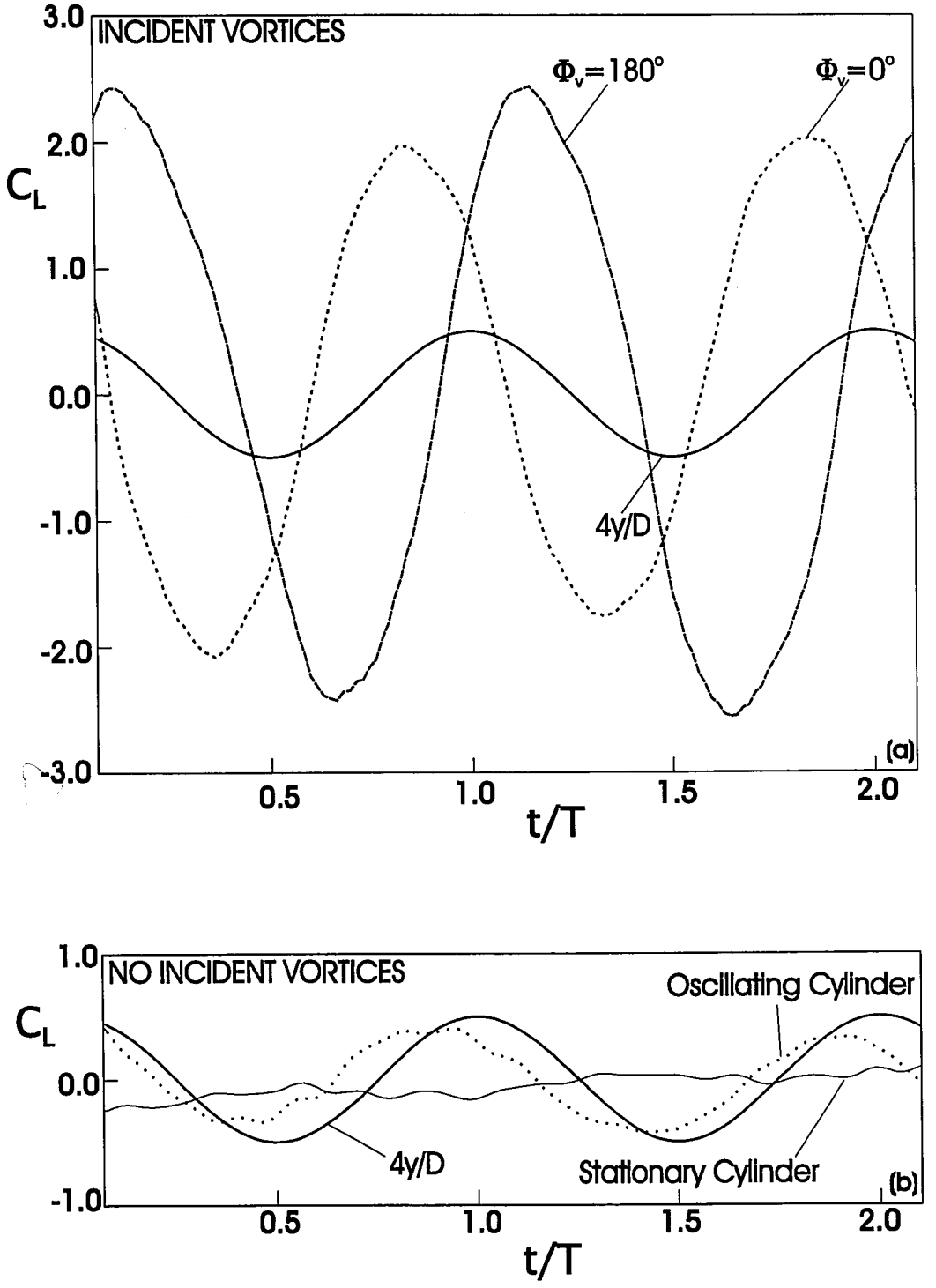

Figure 3.3 Lift coefficient as a function of time for a) incident vortex case, and b) no incident vortex case.

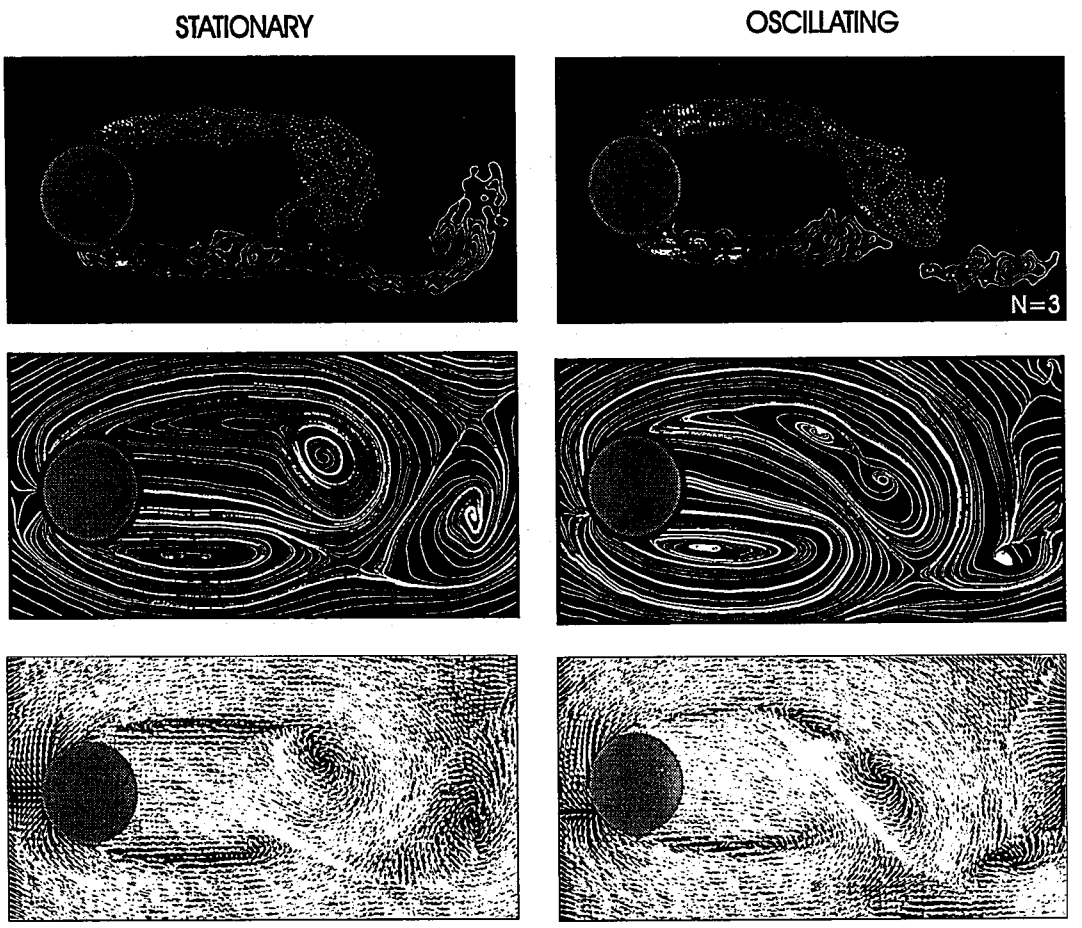

Figure 3.4 Comparison of stationary and oscillating cylinder for no incident vortex cases. Vorticity contours: $\omega_{min} = 2\ s^{-1}$, $\Delta\omega = 1\ s^{-1}$, streamline patterns and velocity vectors: reference frame is moving at 70% of the free stream velocity.

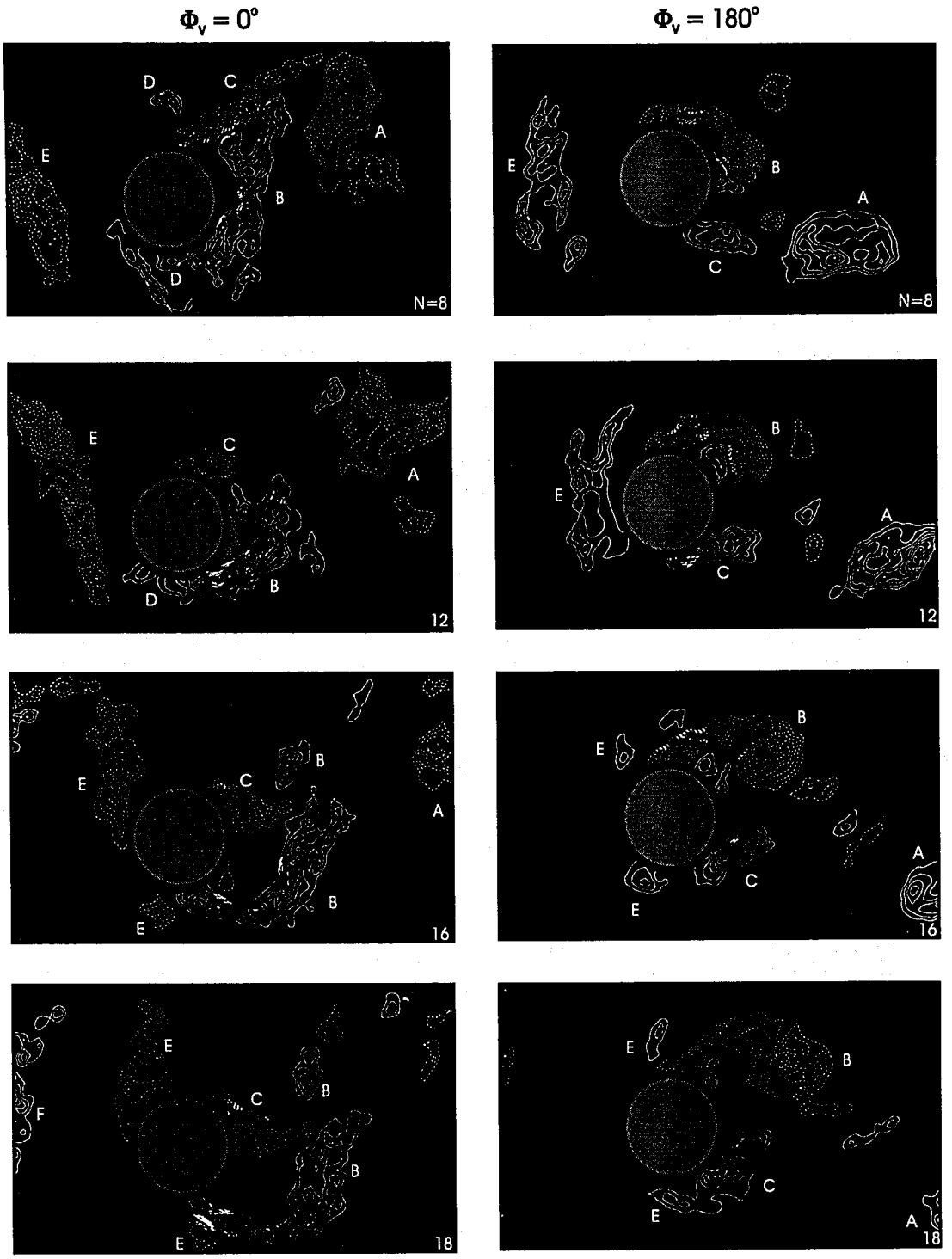

Figure 3.5 Contours of constant vorticity for the incident vortex cases, $\omega_{min} = 2\ s^{-1}$, $\Delta\omega = 1 s^{-1}$.

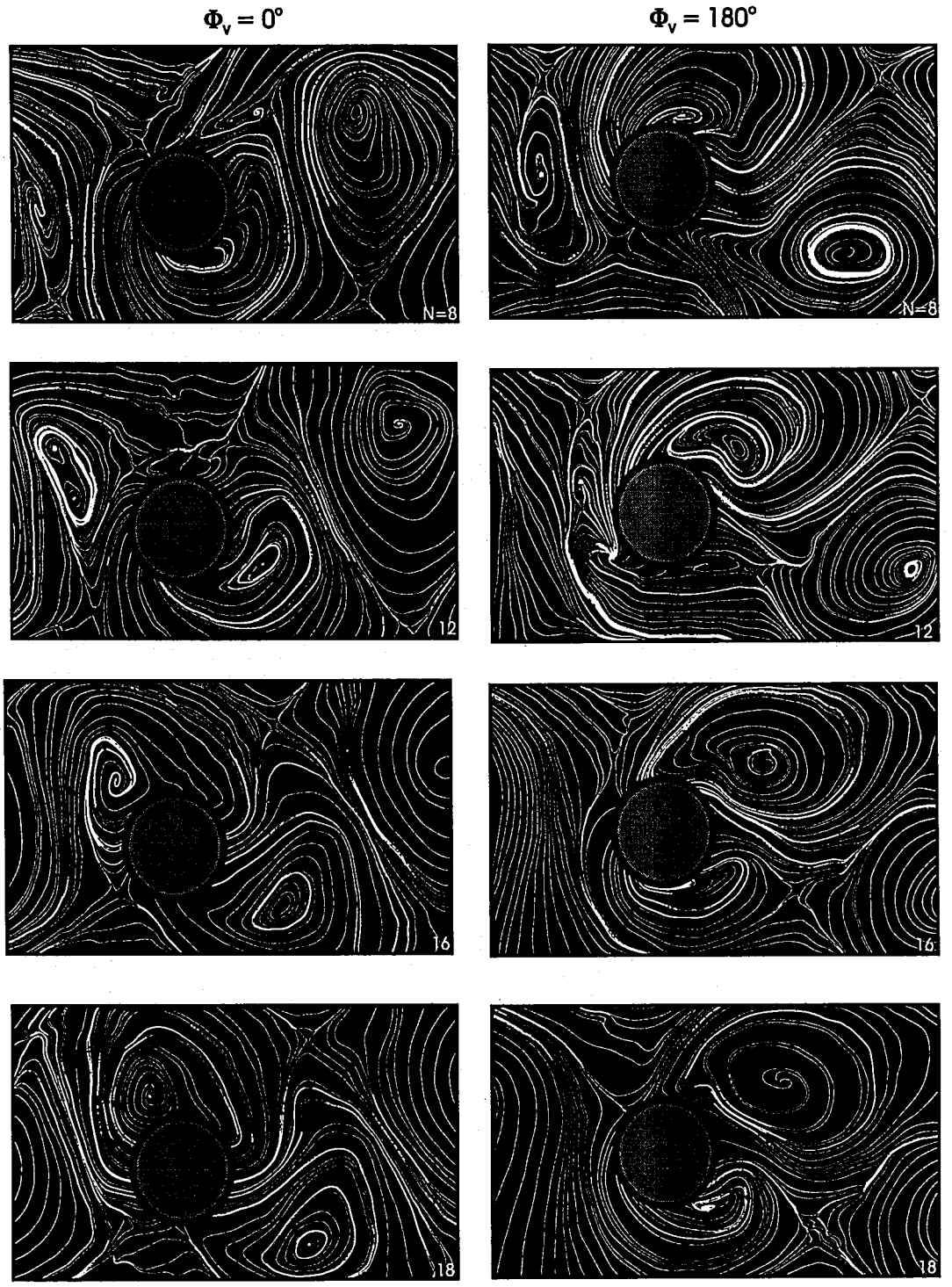

Figure 3.6 Streamline patterns for incident vortex cases in a reference frame moving at 70% of the free stream velocity.

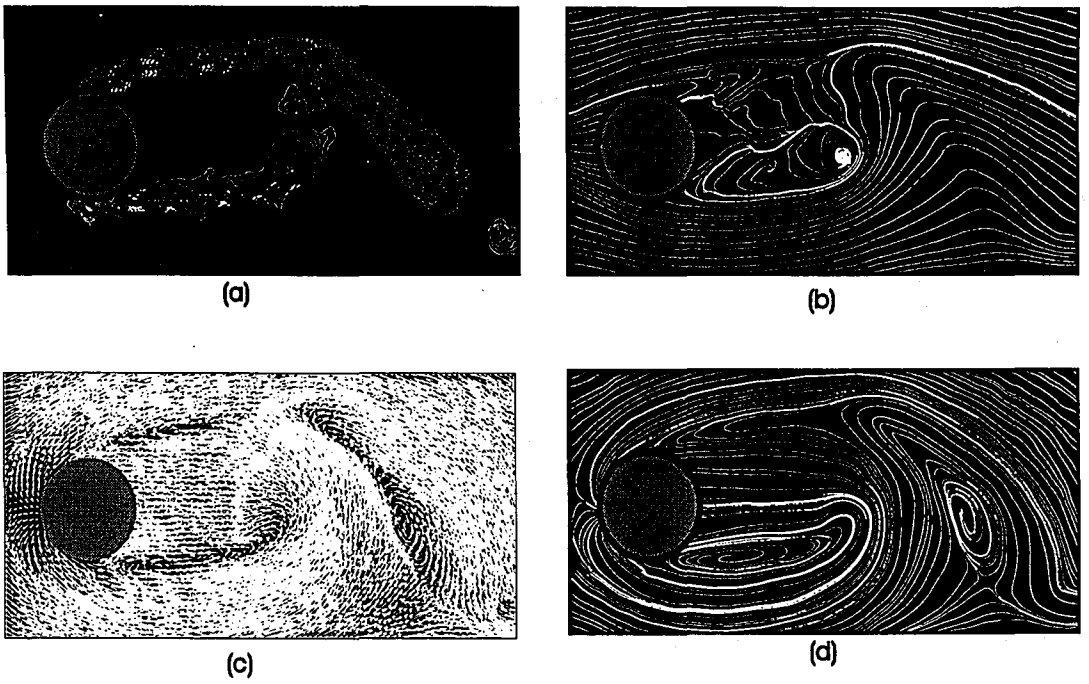

Figure 3.7 Images for no incident vorticity case (N=8).
a) Contours of constant vorticity, $\omega_{min} = 2\ s^{-1}$, $\Delta\omega = 1\ s^{-1}$
b) Stream line pattern in the laboratory reference frame
c) Velocity vector plot in a reference frame moving at 70% of the free stream velocity
d) Streamline pattern in a reference frame moving at 70% of the free stream velocity

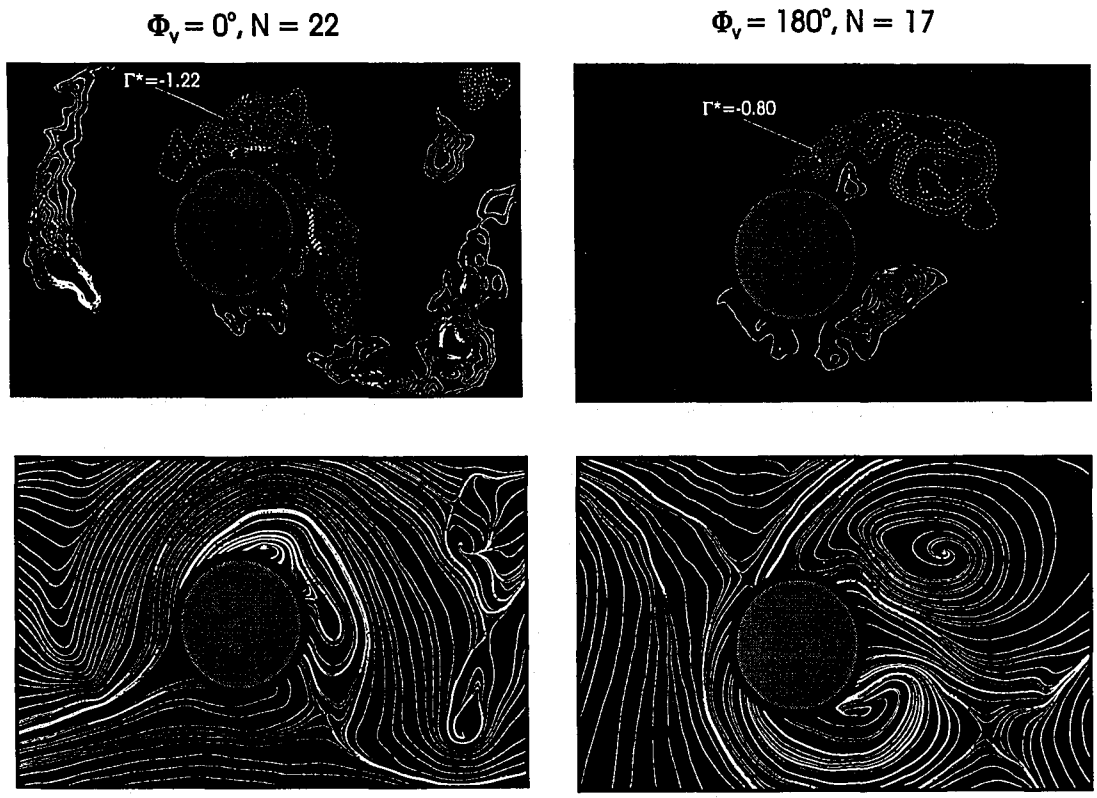

Figure 3.8 Comparison of large vortices formed when incident and shed vorticity concentrations merge. Vorticity contours: $\omega_{min} = 2\ s^{-1}$, $\Delta\omega = 1\ s^{-1}$, Streamline patterns: reference frame is moving at 70% of the free stream velocity.

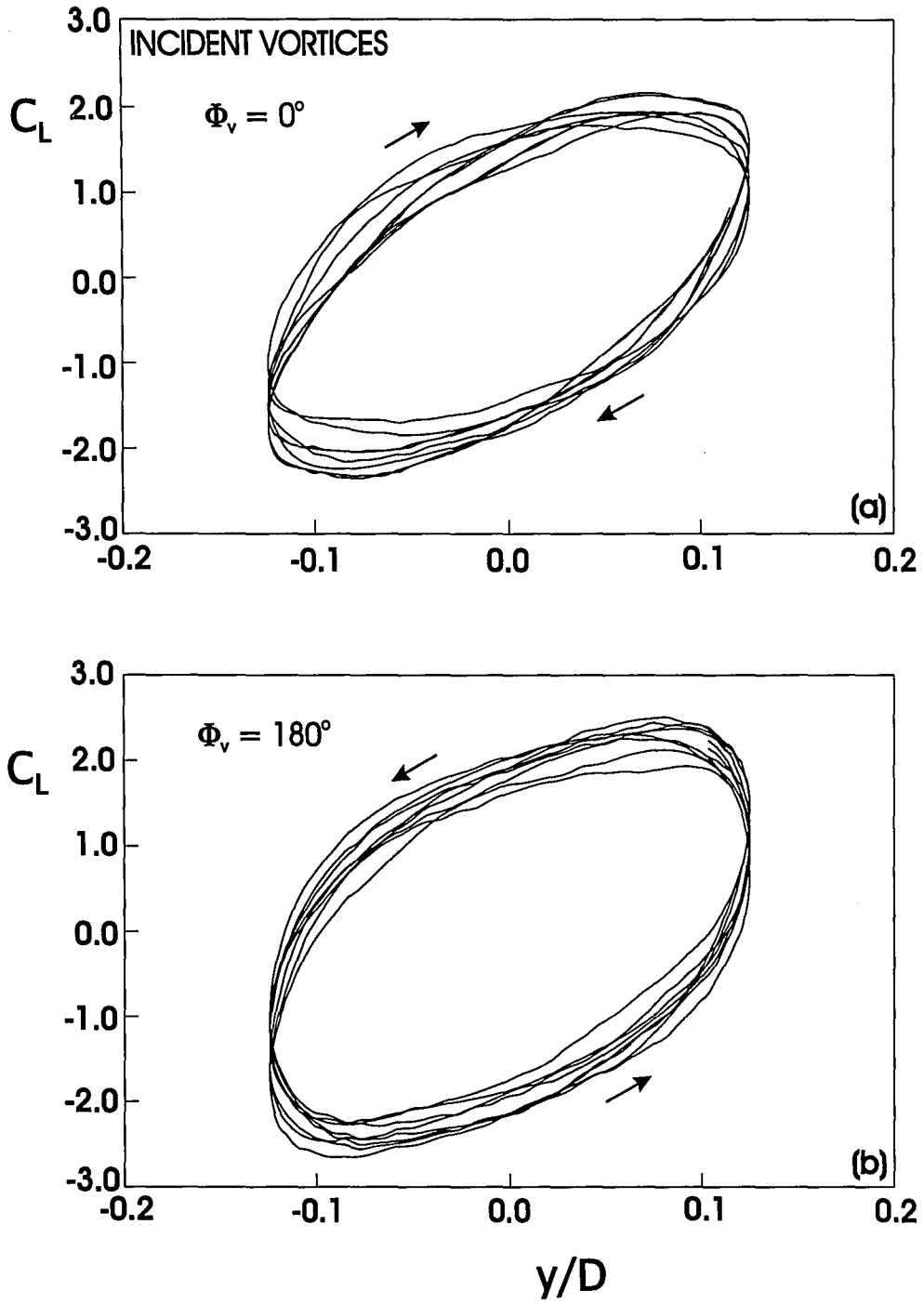

Figure 3.9 Lift phase diagrams for the incident vortex cases.

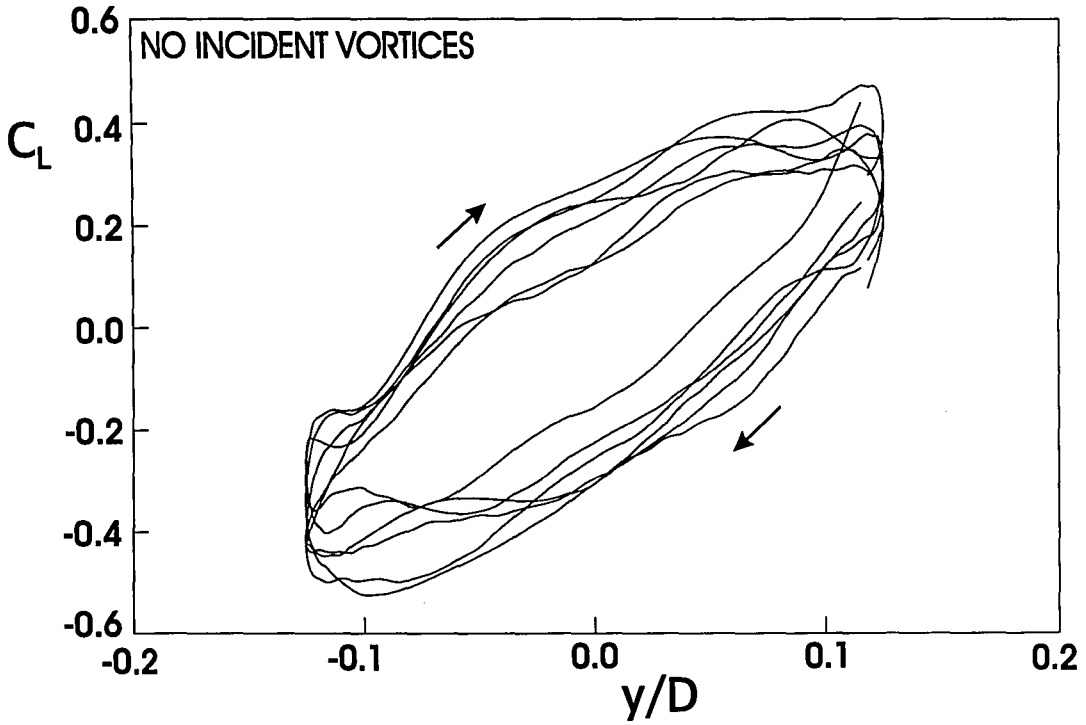

Figure 3.10 Lift phase diagram for the no incident vortex case.

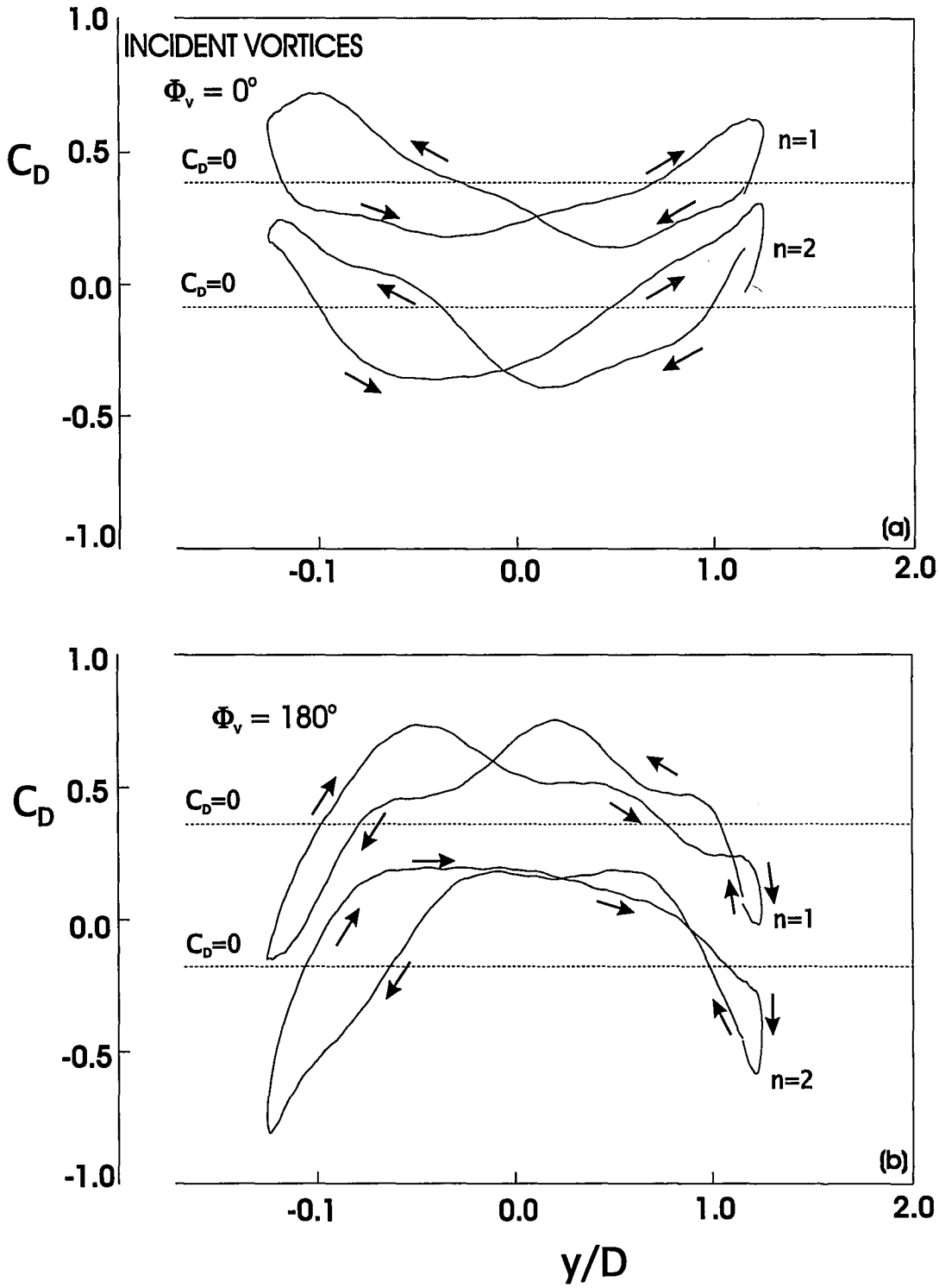

Figure 3.11 Drag phase diagrams for incident vortex cases.

4.0 CONCLUSIONS

This study focused on the flow physics and fluid loading associated with tandem cylinder arrangements in cross flow. The effect of the phase of the downstream cylinder motion, relative to the phase of the incident vortex street, has been investigated. The findings described herein have implications for the design of heat exchangers, offshore structures, or any other configuration for which the vibration of tandem structures in cross-flow is of concern.

It has been shown that there is a large increase in the amplitude of the fluctuating lift coefficient for a tandem cylinder arrangement when compared with a single oscillating cylinder. Depending upon the phase of the vortex street incident upon the downstream cylinder, the amplitude of the fluctuating lift coefficient can increase from 500% to 1000%. PIV images show that the vortex formation length shortens dramatically with the presence of the incident vortical flow. This shortening of the vortex formation length is associated with an increase in the vorticity-induced loading on the cylinder. The change in the fluctuating lift coefficient associated with the relative phase of the incident vorticity for the two tandem cylinder cases is on the order of 50%. The optimization of the relative phase could allow for higher factors of safety and for an extended life span for components subject to this type of loading.

Two distinctly different states of interaction have been shown to exist for cylinders in tandem, depending upon the phase of the incident vortex street relative to the cylinder motion. One state exists, designated as $\Phi_v = 0°$, in which the incident vortex

moves to one side of the cylinder and merges with like-sign vorticity being shed from the cylinder. In this case, the incident vortex remains intact until it merges with the shed vorticity. The two like-sign vortices merge to form a large vortex that has a circulation that is roughly the sum of that for each vortex separately. Another state exists, designated as $\Phi_v = 180°$, in which the incident vortex directly impacts upon the cylinder and breaks up. Part of the total vorticity moves to each side of the cylinder and interacts with the shed vorticity. The circulation of the resulting large vortex is on the order of 60% of that in the $\Phi_v = 0°$ case.

The PIV results show that the vorticity shed in the wake of the downstream cylinder was shifted by approximately 180° for the two incident vortex cases. The $\Phi_v = 0°$ case was similar in phase to the single oscillating cylinder case, while the $\Phi_v = 180°$ case was approximately 180° out-of-phase with these two cases. In the $\Phi_v = 180°$ case, for the same point in the cylinder motion, the vortex shedding took place on the opposite side of the cylinder compared with the single cylinder and $\Phi_v = 0°$ cases. This change in phase indicates that the incident vorticity controls the vortex shedding. This contrasts with the case for the single oscillating cylinder, for which the acceleration of the cylinder controls the phase of the vortex shedding.

The phase diagrams for both tandem cylinder cases and the single oscillating cylinder case exhibit a behavior that is consistent with the results presented for the phase of the shed vorticity. The no incident vortex case and the $\Phi_v = 0°$ case have phase diagrams with clockwise trajectories, indicating that there is an energy transfer from the

fluid to the body. The phase diagram for the $\Phi_v = 180^\circ$ case has a trajectory that is counterclockwise, indicating that there is energy being transferred from the body to the fluid.

Insight has been gained into the effects of the phase of the cylinder motion relative to the phase of the incident vortex street; however, several other issues have arisen as a result of this study. It has been shown that the vortex formation length decreases significantly in the presence of an incident vortex street, which in turn affects the loading on the cylinder. The flow physics that give rise to this reduced vortex formation length are still not clear. It may be a result of an inviscid induction due to the incident vortices, or an alteration of the vorticity in the boundary layer. Another issue is the timing of the vortex shedding from the downstream cylinder for the $\Phi_v = 180^\circ$ case. The phase diagram for the drag coefficient shows an unexpected third loop in the phase trajectory, indicating an irregular occurrence in the wake. Further examination of a time-resolved sequence of high resolution PIV images should provide further insight into this issue.

REFERENCES

Adrian, R.J., "An Image Shifting Technique to Resolve Directional Ambiguity in Double-Pulsed Laser Velocimetry", *Applied Optics*, vol. 25, 1986, pp. 3855-3858.

Adrian, R.J., "Particle-Imaging Techniques for Experimental Fluid Mechanics", *Annual Review of Fluid Mechanics*, vol. 23, 1991, pp. 261-304.

Bearman, P.W., Downie, M.J., Graham, J.M.R., and Obusaju, F.D., "Forces on Cylinders in Viscous Oscillatory Flow at Low Keulegan-Carpenter Numbers", *Journal of Fluid Mechanics*, vol. 154, 1985, pp. 337-356.

Bishop, R.E.D. and Hassan, A.Y., "The Lift and Drag Forces on a Circular Cylinder in a Flowing Fluid", *Proceedings of the Royal Society (London)*, Series A, vol. 277, 1964, pp. 51-75.

Cetiner, O.N., Personal Communication, 1996.

Chyu, C.K. and Rockwell, D., "Near-Wake Structure of an Oscillating Cylinder: Effect of Controlled Shear-Layer Vortices", *Journal of Fluid Mechanics*, vol. 322, 1996, pp. 21-49.

Corcoran, T., "Control of the Wake from a Simulated Blade by Trailing-Edge Blowing", Masters Thesis, Lehigh University, 1992.

Gopalkrishnan, R., Triantafyllou, M.S., Triantafyllou, G.S., and Barrett, D., "Active Vorticity Control in a Shear Flow Using a Flapping Foil", *Journal of Fluid Mechanics*, vol. 274, 1994, pp. 1-21.

Hammache, M. and Gharib, M., "An Experimental Study of the Parallel and Oblique Vortex Shedding from Circular Cylinders", *Journal of Fluid Mechanics*, vol. 232, 1991, pp. 567-590.

Jefferies, R.W. and Rockwell, D., "Interactions of a Vortex with a Leading Edge", *AIAA Journal*, vol. 34(11), 1996, pp. 2448-2450.

Keane, R.D. and Adrian, R.J., "Theory of Cross-Correlation Analysis of PIV Images", *Applied Scientific Research*, vol. 49(3), 1992, pp. 191-215.

Kiya, M., Arie, M., Tamura, H., and Mori, H., "Vortex Shedding from Two Circular Cylinders in Staggered Arrangement", *Transactions of the ASME, Journal of Fluids Engineering*, vol. 102, 1980, pp. 166-173.

Landreth, C.C. and Adrian, R.J., "Measurement and Refinement of Veloctiy Data Using High Image Density Analysis in Particle Image Velocimetry", *Applications of Laser Anemometry: Proceedings of the 4th International Symposium*, edited by R.J. Adrian, T. Asunuma, D. Durao, F. Durst, and J. Whitlaw, Springer Verlag, Berlin, 1989, pp. 484-497.

Lin, J.-C., "NFILV", software, Fluid Mechanics Lab., Lehigh University, 1994.

Lin, J.-C., "BOUND2" software, Fluid Mechanics Lab., Lehigh University, 1996.

Lin, J.-C., Towfighi, J., and Rockwell, D., "Instantaneous Structure of the Near-Wake of a Circular Cylinder: On the Effect of Reynolds Number", *Journal of Fluids and Structures*, vol. 9, 1995, pp. 409-418.

Magness, C., "Streaming Function Generator, SFG", software, Fluid Mechanics Lab., Lehigh University, 1990.

Magness, C., and Troiano, J., "Automatic Laboratory Technician, ALT", software, Fluid Mechanics Lab., Lehigh University, 1991.

Mahir, N. and Rockwell, D., "Vortex Formation from a Forced System of Two Cylinders, Part 1: Tandem Attangement", *Journal of Fluids and Structures*, vol. 10, 1996, pp. 473-489.

Naudascher, E. and Rockwell, D., *Flow-Induced Vibrations: An Engineering Guide*, Balkema, Rotterdam, 1994.

Ongoren, A. and Rockwell, D., "Flow Structure from an Oscillating Cylinder, Part 1: Mechanisms of Phase shift and Recovery in the Near-Wake", *Journal of Fluid Mechanics*, vol. 191, 1988, pp. 197-223.

Paidoussis, M.P., "Fluidelastic Vibration of Cylinder Arrays in Axial and Cross-Flow: State of the Art", *Journal of Sound and Vibration*, vol. 76(3), 1981, pp. 329-360.

Raffel, M. and Kompenhans, J., "Theoretical and Expermental Aspects of Image Shifting by Means of a Rotating Mirror System for Particle Image Velocimetry", *Measurement Science Technonogy*, vol. 6, 1995, pp. 795-808.

Rayleigh, L., *Theory of Sound*, 2nd ed., Dover, New York, 1945.

Richardson, E.G., "Aeolian Tones", *Proceedings of the Physical Society of London*, vol. 36, 1923, pp. 153-167.

Robinson, O., "V3", software, Fluid Mechanics Lab., Lehigh University, 1992.

Rockwell, D., Magness, C., Robinson, O., Towfighi, J., and Corcoran, T., "High Image-Density Particle Image Velocimetry Using Scanning Techniques", *Experiments in Fluids*, vol. 14, 1993, pp. 181-192.

Schiller, L. and Linke, W., "Pressure and Frictional Resistance of a cylinder at Reynolds Numbers from 5,000 to 40,000", *NACA Technical Memorandum*, No. 715, July 1933.

Seke, E., "PIV3", software, Fluid Mechanics Lab., Lehigh University, 1993.

Streitlien, K., Triantafyllou, G.S., and Triantafyllou, M.S., "Efficient Foil Propulsion Through Vortex Control", *AIAA Journal*, vol. 34(11), 1996, pp. 2315-2319.

Thomlinson, E., *Strain Gage Stings*, Fluid Mechanics Lab., Lehigh University, 1996.

Tritton, D.J., "Experiments on the Flow Past a Circular Cylinder at Low Reynolds Numbers", *Journal of Fluid Mechanics*, vol. 6, 1959, p. 547.

Weaver, D.S., and Fitzpatrick, J.A., "A Review of Cross-Flow Induced Vibrations in Heat Exchanger Tube Arrays", *Journal of Fluids and Structures*, vol. 2, 1988, pp. 73-93.

Williamson, C.H.K., "Oblique and Parallel Modes of Vortex Shedding in the Wake of a Circular Cylinder at Low Reynolds Numbers", *Journal of Fluid Mechanics*, vol. 206, 1989, pp. 574-627.

Williamson, C.H.K. and Roshko, A., "Vortex Formation in the Wake of an Oscillating Cylinder", *Journal of Fluids and Structures*, vol. 2, 1988, pp. 355-381.

Zaida, S. and Ongoren, A., "Vorticity Shedding and Acoustic Resonance in an In-Line Tube Bundle, Part 1: Vorticity Shedding", *Journal of Fluids and Structures*, vol.6, 1992, pp. 271-292.

Zaida, S. and Ongoren, A., "Vortex Shedding in a In-Line Tube Bundle with Large Tube Spacings", *Journal of Fluids and Structures*, vol. 7, 1993, pp. 661-687.

Zdravkovich, M.M., "review of Flow Interference Between Two Circular Cylinders in Various Arrangements", *Transactions of the ASME, Journal of Fluids Engineering*, vol. 99, 1977, pp. 618-633.

Zdravkovich, M.M., "The Effects of Interference Between Circular Cylinders in Cross-Flow", *Journal of Fluids and Structures*, vol. 1, 1987, pp. 239-261.

Zdravkovich , M.M. and Pridden, D.L., "Interference Between Two Circular Cylinders; Series of Unexpected Discontinuities", *Journal of Industrial Aerodynamics*, vol. 2, 1977, pp. 255-270.

APPENDICES

Appendices A and B contain raw data which were considered to be too extensive to be included in the main body of this thesis. Highly resolved time sequences of one half cycle of cylinder motion are included for the incident vortex cases at a Reynolds number of 700, as well as short time sequences for the no incident vortex cases. Raw force traces, which have not yet been digitally filtered, are also included. A second set of experimental data is included for similar tests performed at a Reynolds number of 4500. This information was excluded from the main body of this thesis because there were some questions about the lock-on of the vortex shedding from the downstream cylinder.

APPENDIX A:

Reynolds Number = 700

The following images (figures A-1 and A-2) are time sequences of contours of constant vorticity for the no incident vortex and incident vortex cases for a Reynolds number of 700. In these cases the vorticity levels were different from those used in chapter 3, so the reader should only compare these images qualitatively. The minimum vorticity contour in all of these cases is at $\omega = 2\ s^{-1}$ and $\Delta\omega = 2\ s^{-1}$. The small scale structures have not been filtered from these images as they were in chapter 3. The time resolution of thesis images is $\Delta t/T = 0.033$. The notation for these is as follows: 'ss' denotes the single-stationary cylinder case (no incident vortex, stationary); 'so' denotes the single-oscillating cylinder case (no incident vortex, oscillating); 'min' denotes the $\Phi = 0^{\circ}$ incident vortex case (L = 155 mm); and 'max' denotes the $\Phi = 180^{\circ}$ incident vortex case (L = 113 mm).

One sample plot of raw lift coefficient as a function of time (figure A-3) is presented to give an idea of how the unfiltered data looks. For the data presented in chapter 3, the data was digitally filtered with a low-pass cutoff frequency of 1 Hz.

APPENDIX B:

Reynolds Number = 4500

As mentioned previously, a second set of experiments was performed at a Reynolds number of 4500. In this case a different mechanism was used to vary the phase of the cylinder motion relative to the incident vortex street. The cylinders were oscillated at slightly different frequencies, (f_1 = 1.11 Hz. and f_2 = 0.975 Hz) while retaining the same cylinder spacing. The vortices traveled at the same speed for both cases, but the downstream cylinder was at a different phase in its motion when the incident vortex arrived.

A new set of PIV parameters was employed for this new case. The 72 facet rotating mirror operated at 7.5 Hz resulting in a scanning frequency of 540 Hz. There was no unsteadiness in the laser sheet for this scanning frequency, as there had been for the frequency used in the Re = 700 case. A shutter speed of 1/100 and f-stop of 6.3 were used for this case. At this shutter speed, the maximum framing rate was determined to be around 8.8 Hz. ALT was used to command the camera to fire once every 126 ms (each discrete step was 6 ms in this case) for a framing rate of 7.93 Hz. The oscillation period was considerably shorter at this Reynolds number, so only 6-9 frames could be acquired per cycle ($\Delta t/T$ = 0.123 - 0.140). The bias mirror operated at a voltage of 0.325 V and a frequency of 21.7 Hz.

A matrix of tests was performed at this Reynolds number similar to that at the Reynolds number of 700. For both incident vortex cases, the cylinder spacing was 113

mm. Preliminary experiments showed that the fluctuating lift forces varied greatly with relatively small variations in oscillation frequency. The vortex shedding frequency for the stationary cylinder system was measured to be 1.111 Hz (based on the frequency of the measured lift force fluctuations). This oscillation frequency resulted in a relatively small fluctuating lift force amplitude. A slightly lower oscillation frequency (0.975 Hz) produced a significantly larger fluctuating lift force amplitude, so this frequency was used for the second incident vortex case. The attached plot of lift coefficient as a function of time for the two cases (figure B-1) shows the relative amplitudes of the fluctuating lift coefficient for these two cases.

From the time trace of lift coefficient, it can be seen that lock-on was not perfectly attained for the 1.111 Hz case. The phase diagram for this case (figure B-2) also shows some variation from what would be expected for lock-on.

Time sequences of contours of constant vorticity are also presented here (figures B-3 and B-4). The notation for these sequences is as follows: 'stat' denotes the no incident vortex, stationary cylinder case; 'osc' denotes the no incident vortex, oscillating cylinder case (f = 1.21 Hz); '10' denotes the incident vortex case in which the oscillation frequency was 0.975 Hz (T = 1.026 sec); and '9' denotes the incident vortex case in which the oscillation frequency was 1.111 Hz (T = 0.900 sec). One very interesting aspect of the contours of constant vorticity is that for the no incident vortex cases, the vortex formation length decreases dramatically when the cylinder is oscillated.

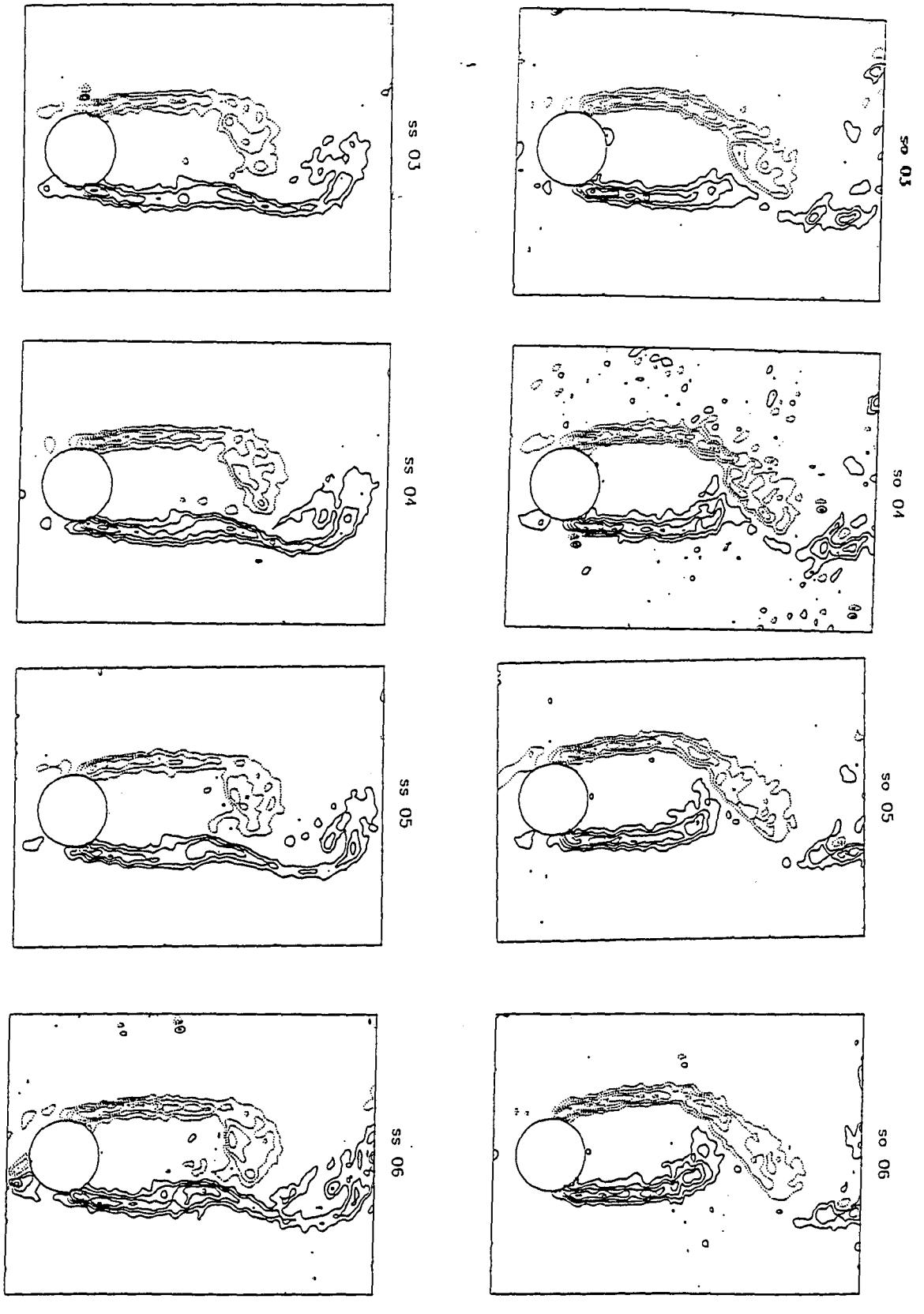

figure A-1 See next page for caption.

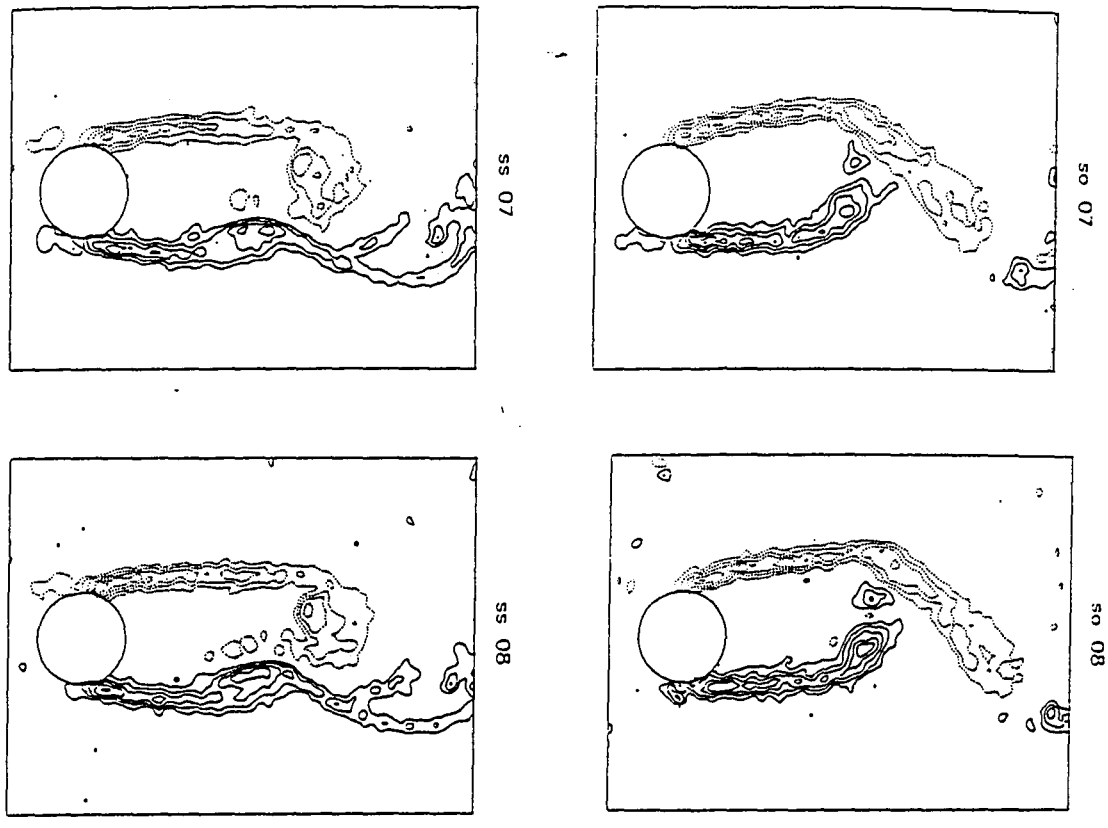

Figure A-1 time sequence of vorticity contours for Re = 700, no incident vortex case.

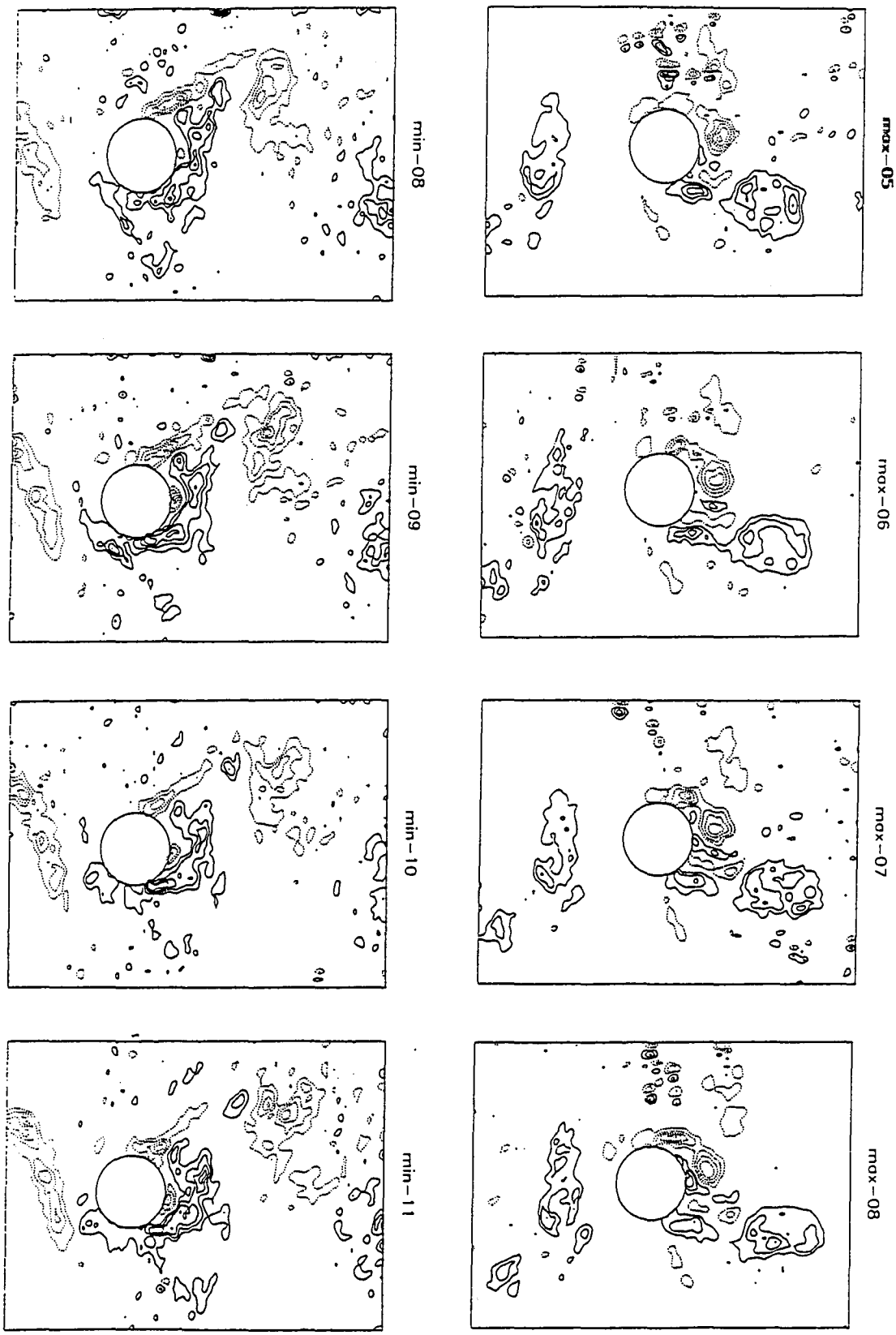

Figure A-2 See page 63 for caption.

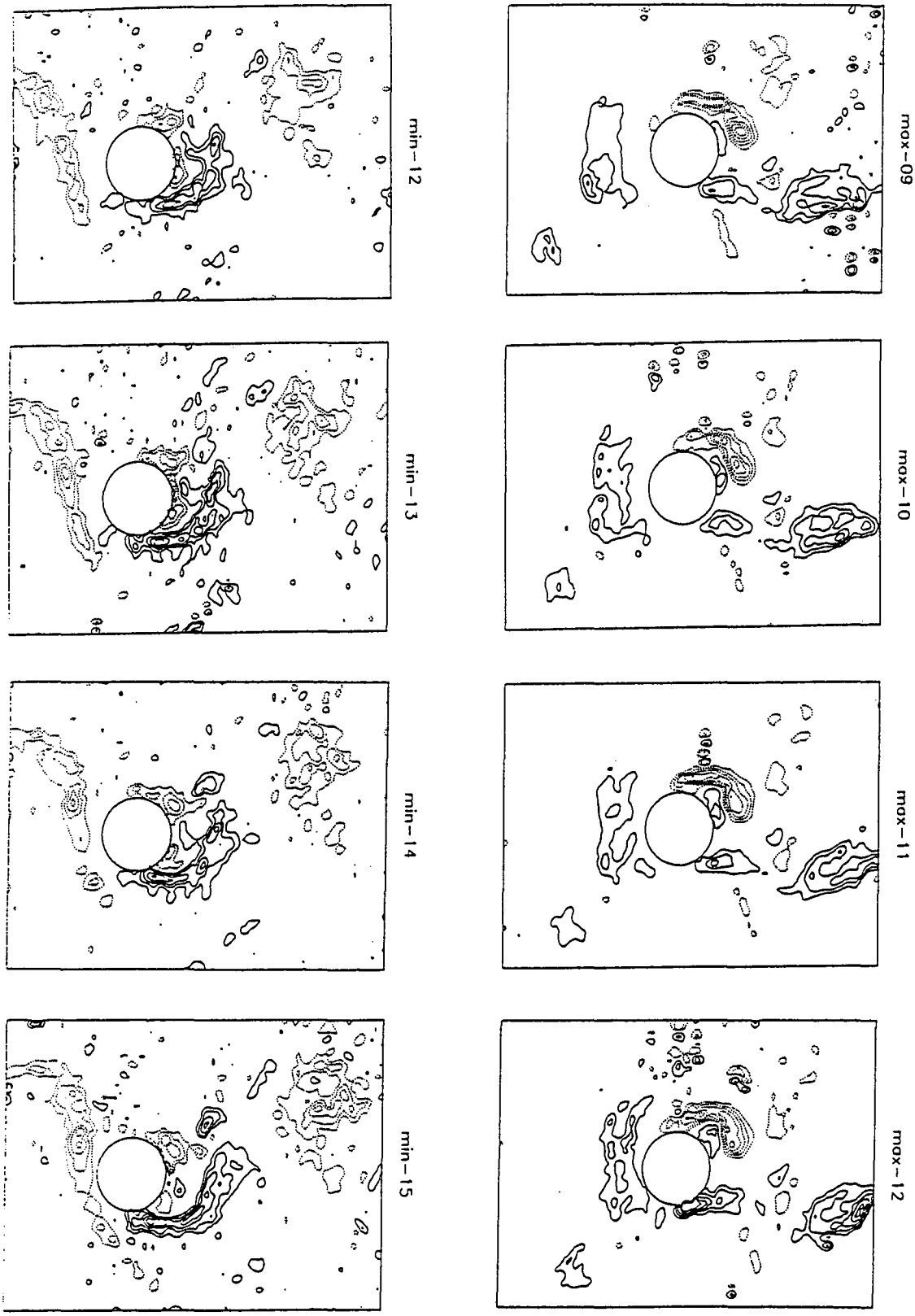

Figure A-2 See page 63 for caption.

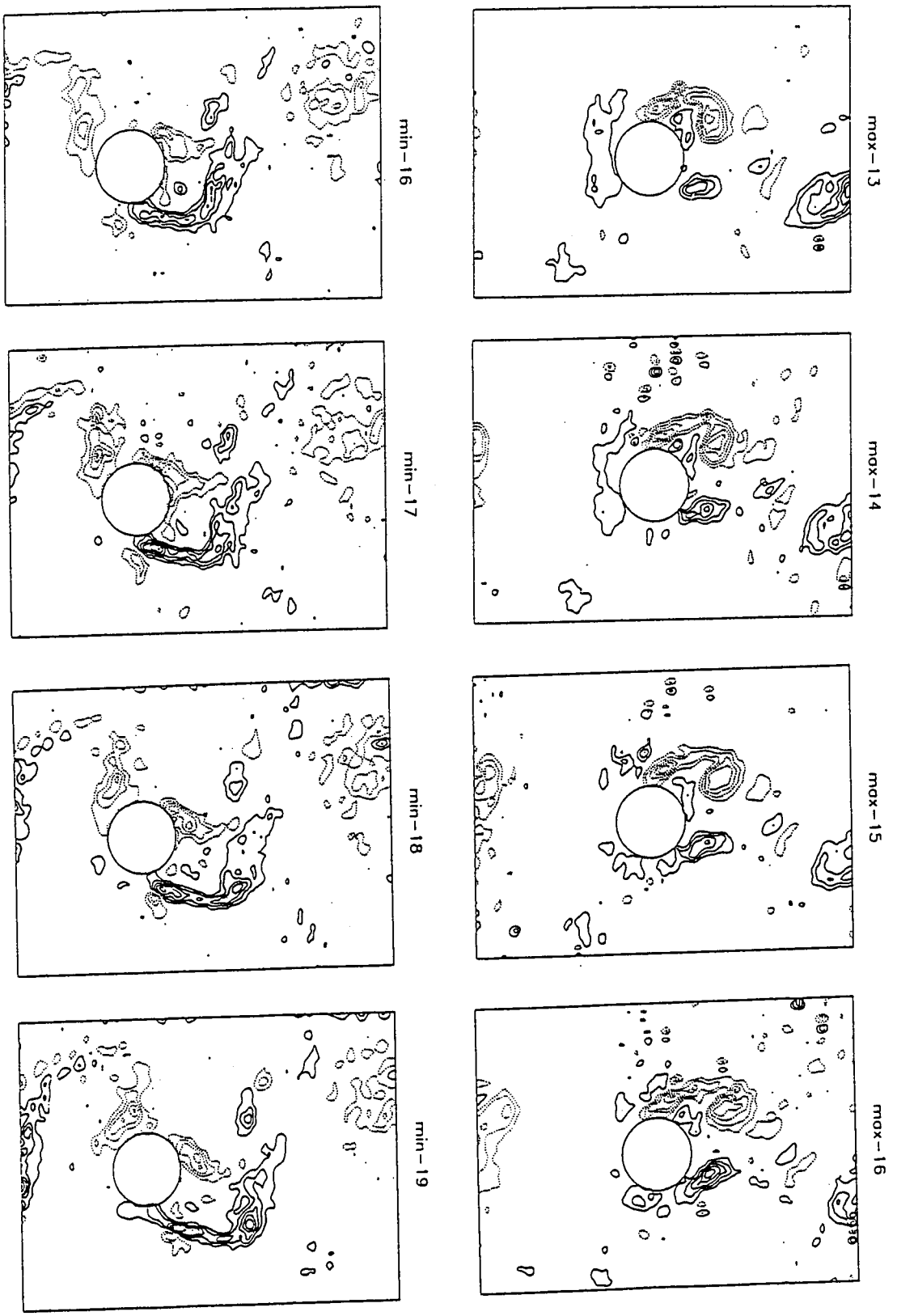

Figure A-2 See page 63 for caption.

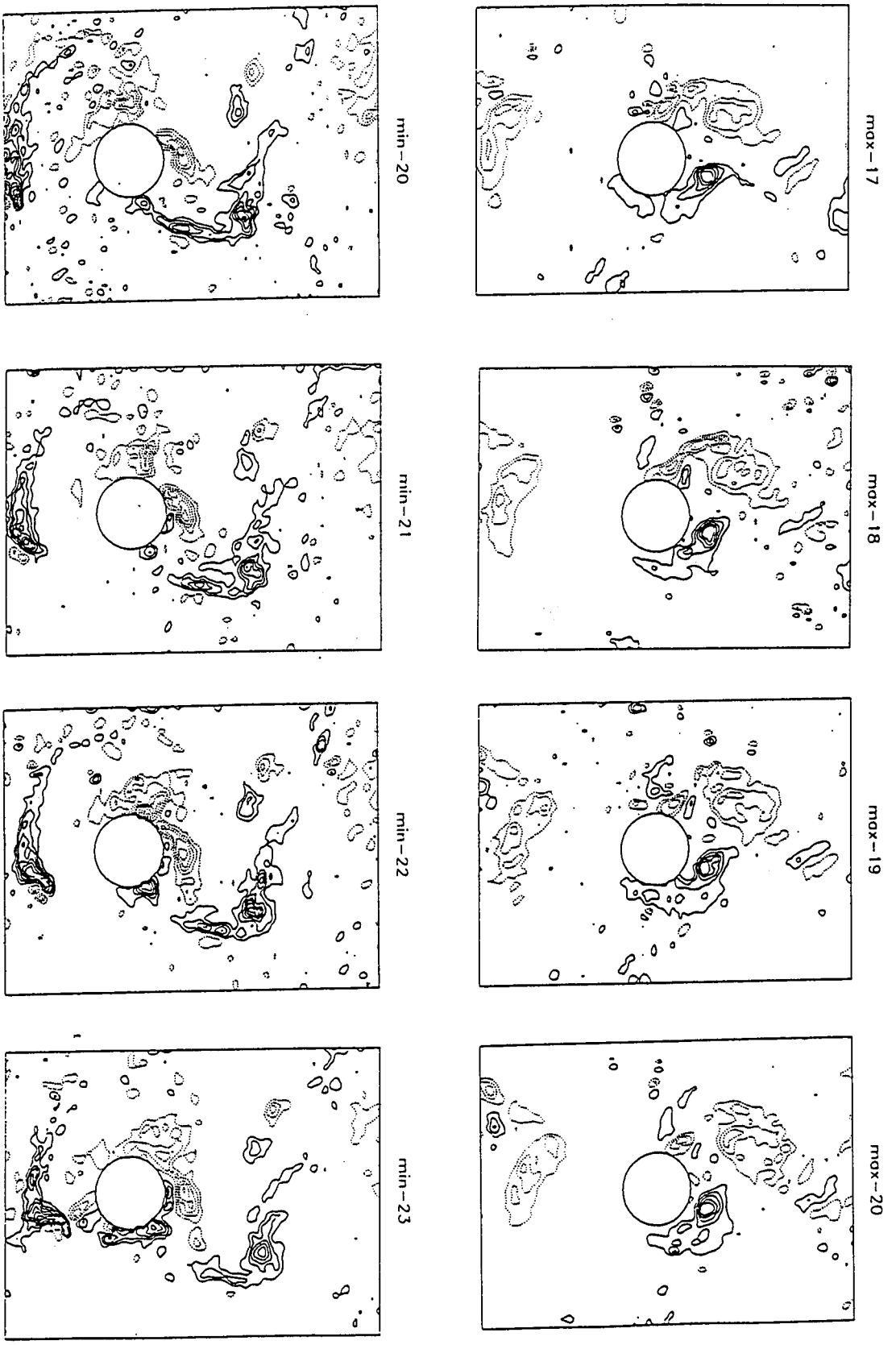

Figure A-2 Time sequence of vorticity contours for Re = 700, incident vortex case.

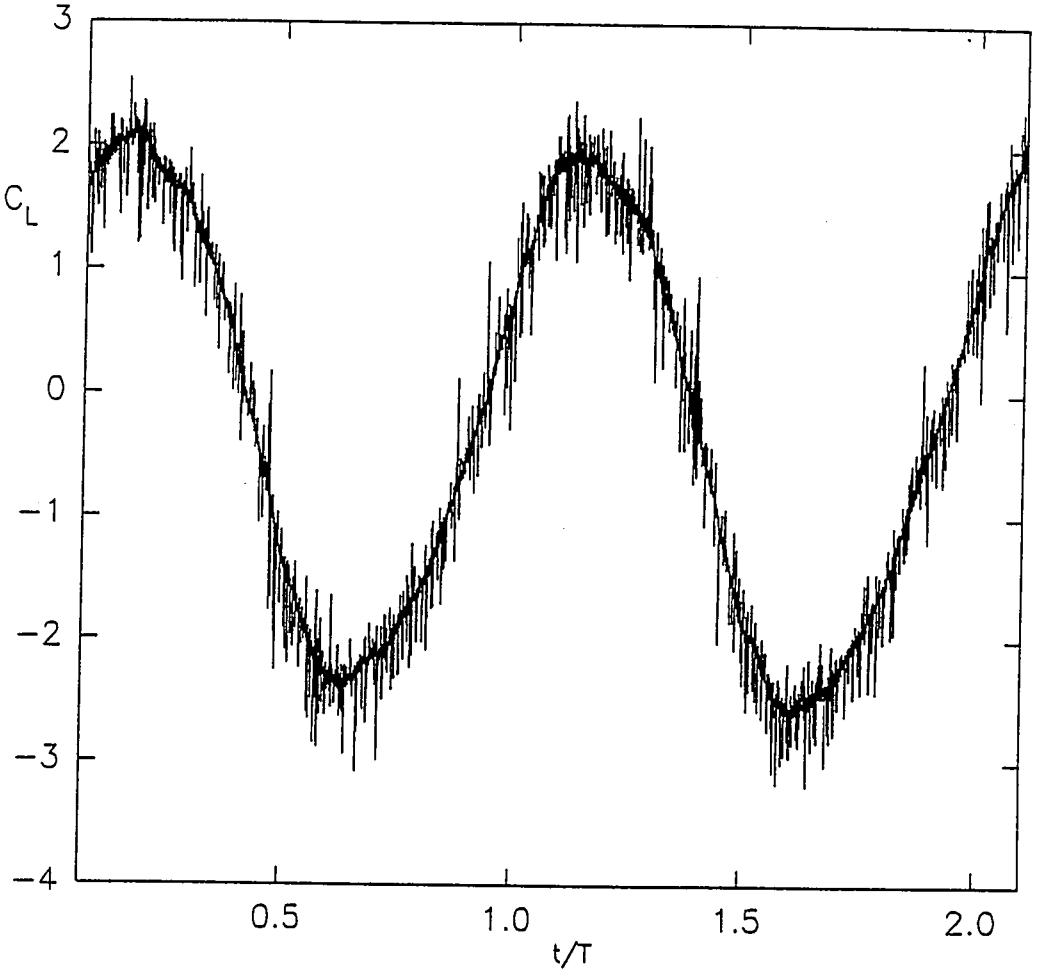

Figure A-3 Unfiltered lift coefficient trace for Re = 700, incident vortex case, $\Phi_v = 180°$.

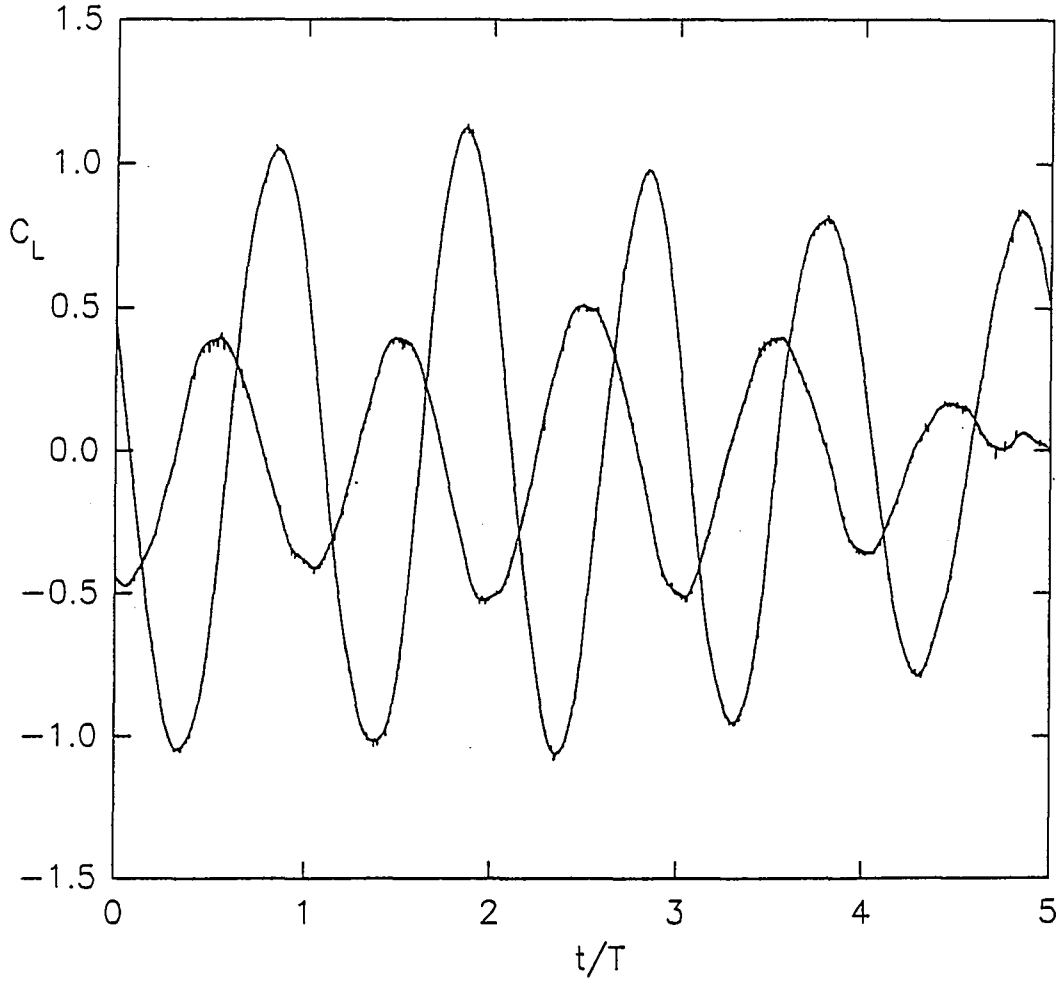

Figure B-1 Lift coefficient time trace for Re = 4500, incident vortex cases.

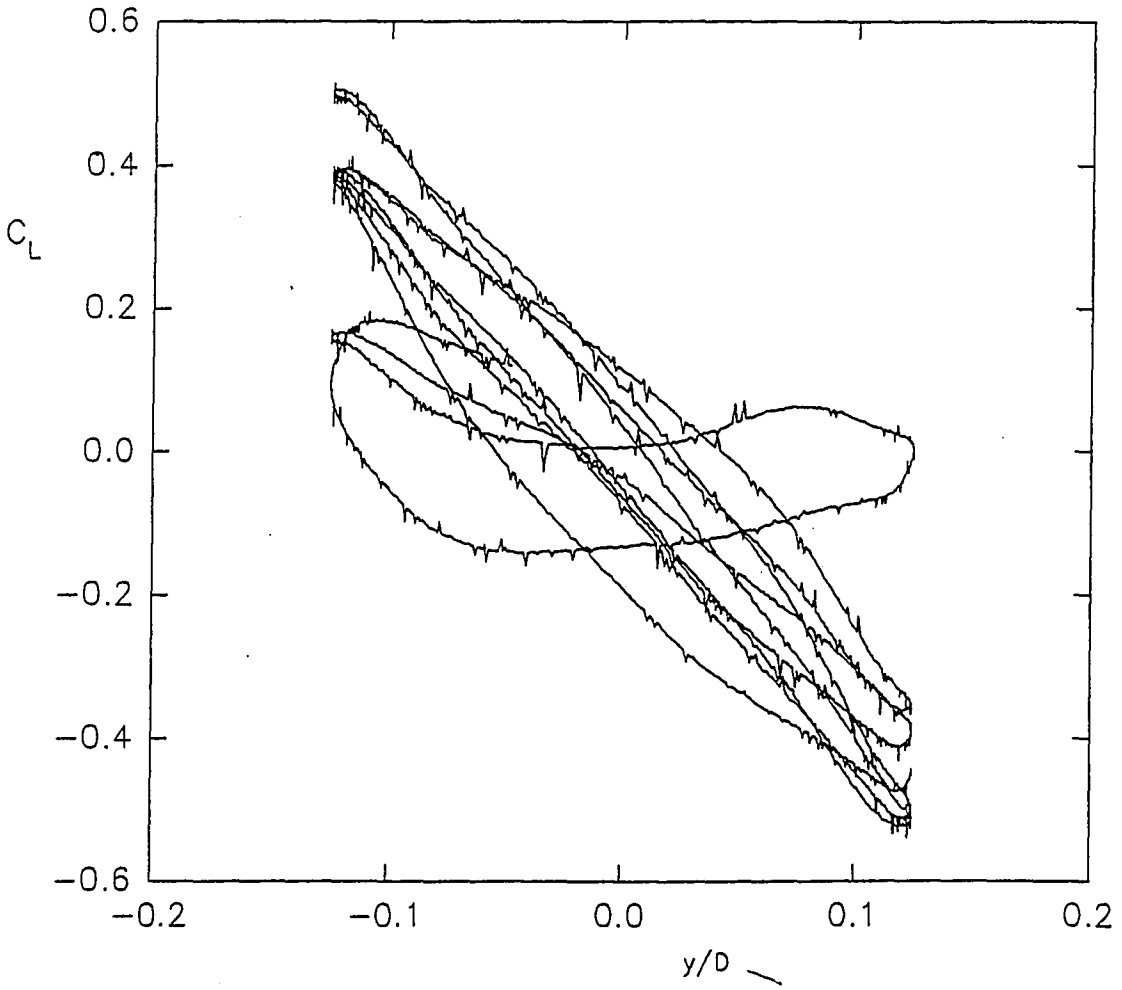

Figure B-2 Lift phase diagram for Re = 4500, incident vortex case, f_e = 1.111 Hz.

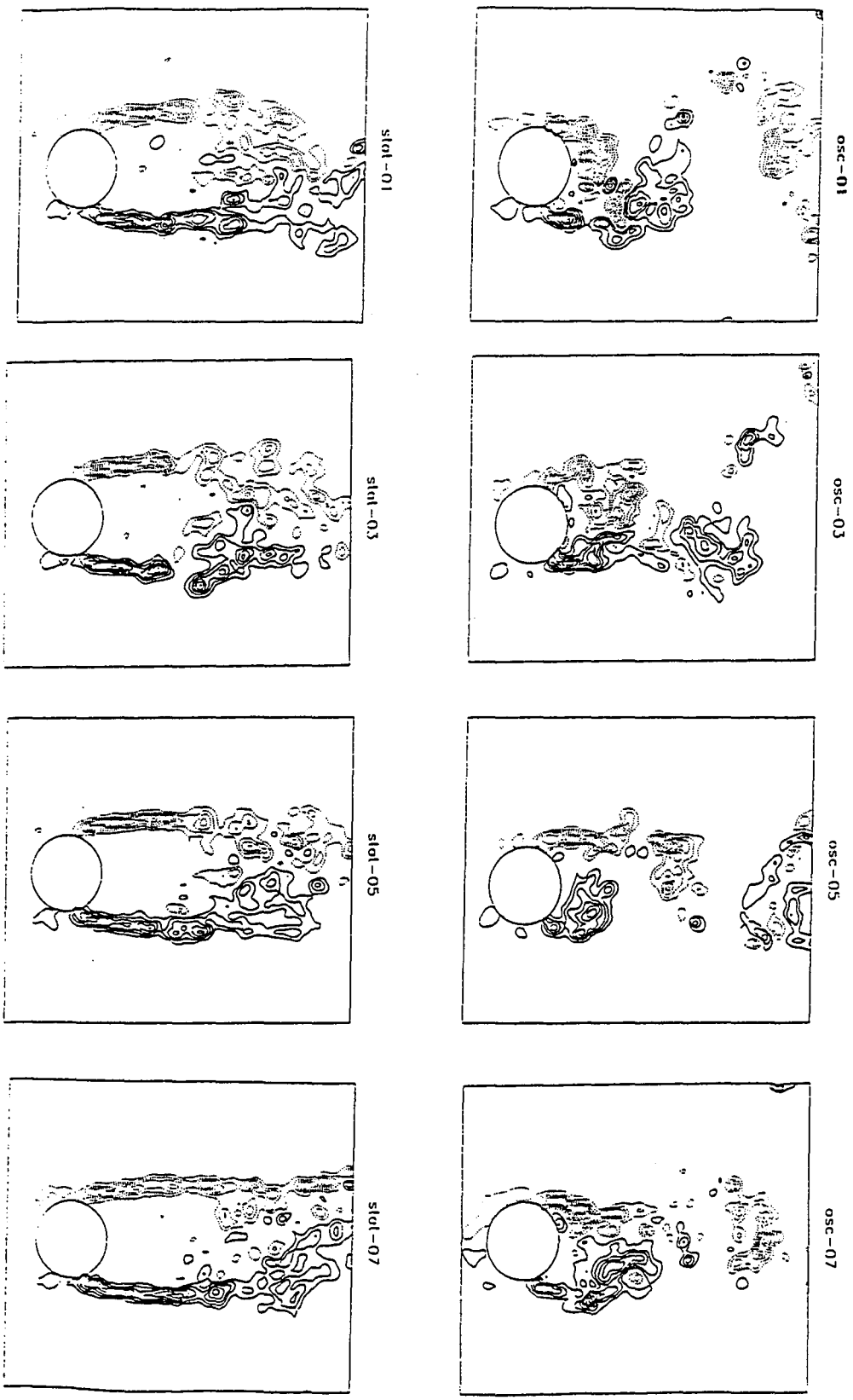

Figure B-3 Time sequence of vorticity contours for Re = 4500, no incident vortex cases.

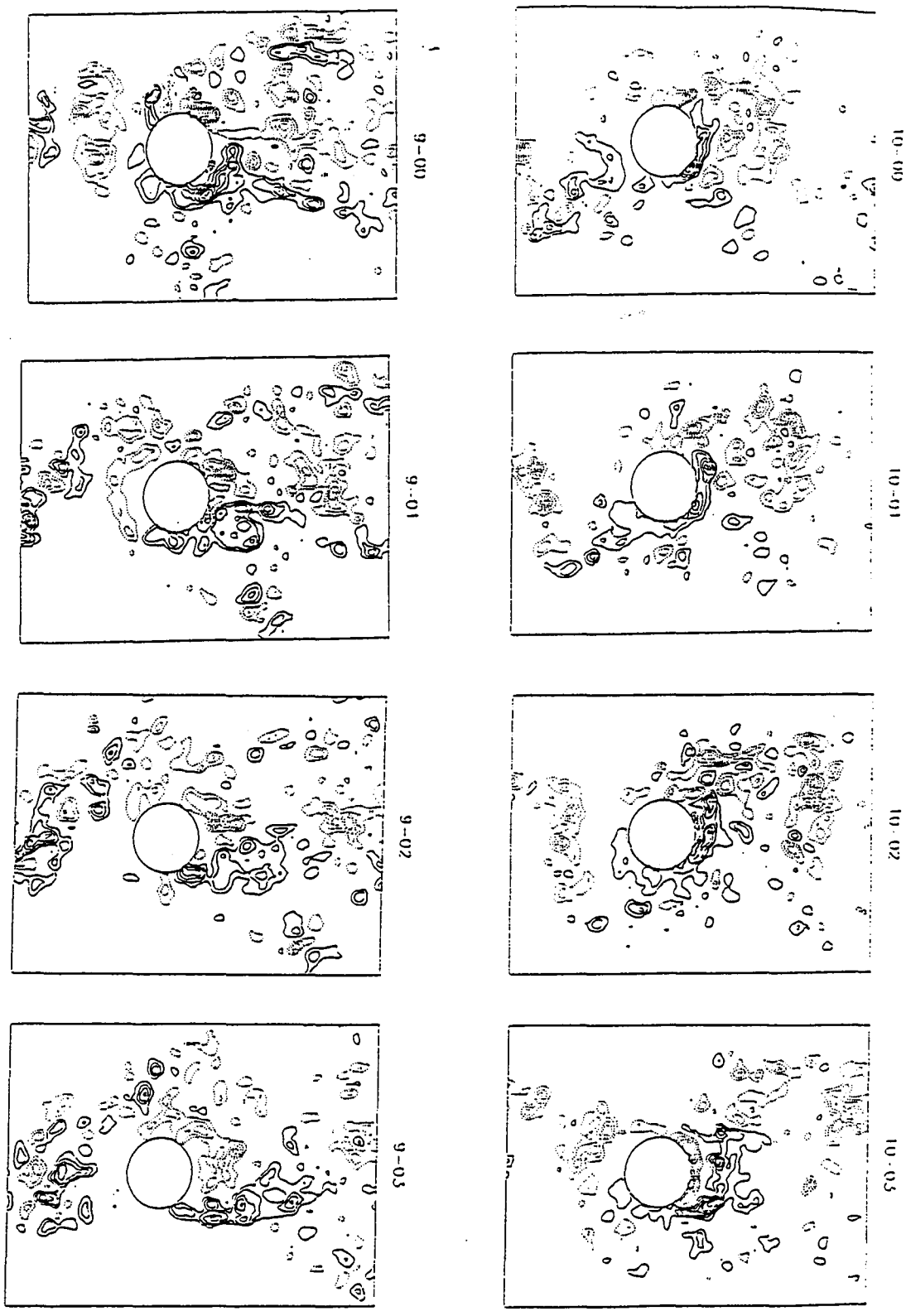

Figure B-4 See page 69 for caption.

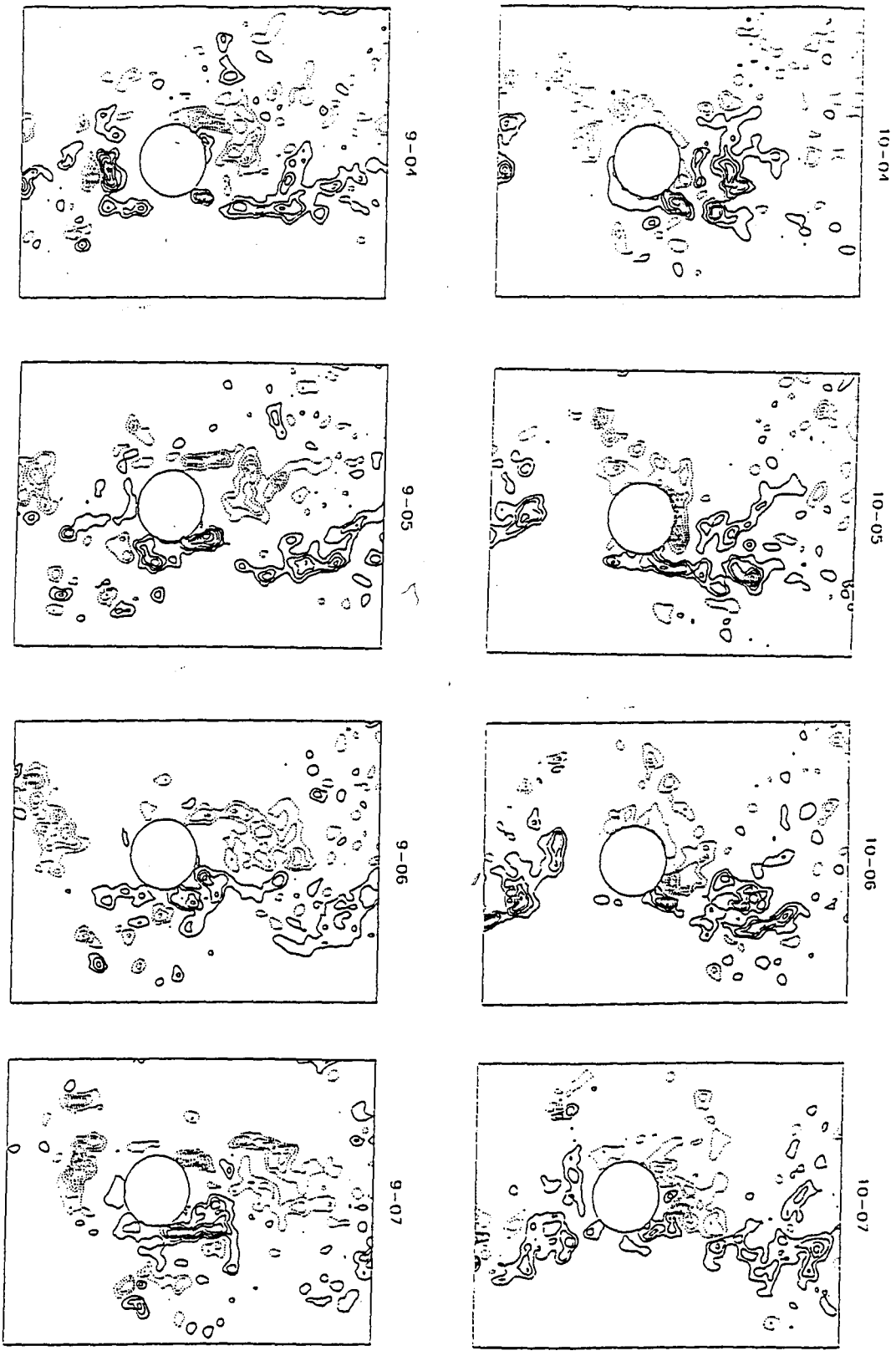

Figure B-4 Time sequence of vorticity contours for Re = 4500, incident vortex cases.

VITA

Matthew Albert Gaydon was born on June 19, 1973 in Muncy Pennsylvania to Lewis P. and Marie M. Gaydon. The author graduated with highest honors from Muncy High School in 1991, where he was the president of the class of 1991. In the fall of 1991, he began studies in mechanical engineering at Bucknell University in Lewisburg, Pennsylvania. In June, 1995, he graduated with a Bachelor of Science degree in Mechanical Engineering in the Honors Program from Bucknell University, and he began graduate studies in mechanical engineering at Lehigh University in Bethlehem, Pennsylvania. He spent time working as a research assistant and as a teaching assistant while at Lehigh. In November, 1995, he presented a paper entitled "The attenuation of flow-induced vibration of a staggered cylinder pair with the use of perforated splitter plates" at the 1995 International Mechanical Engineering Congress and Exposition in San Francisco, CA, and he was awarded the ASME Fluids Engineering Division National Young Engineer Paper Award. The author participated in the I.A.E.S.T.E. exchange program for students, in which he spent the Summer of 1996 working as a research assistant for the Deutsche Forchunsansalt fur Luft- und Raumfahrt (DLR) in Goettingen, Germany. The author's other publications include "Effect of upstream separation geometry on the vibrations of the downstream cylinder of a staggered pair", *Flow-Induced Vibration*, 1995 and "Hybrid stereoscopic particle image velocimetry", *Experiments in Fluids*, accepted for publication March, 1997.

END

OF

TITLE